Cell Reports
Medicine

Article

Distinct viral reservoirs and immune signatures in individuals on long-term antiretroviral therapy with perinatally acquired HIV-1

Graphical abstract

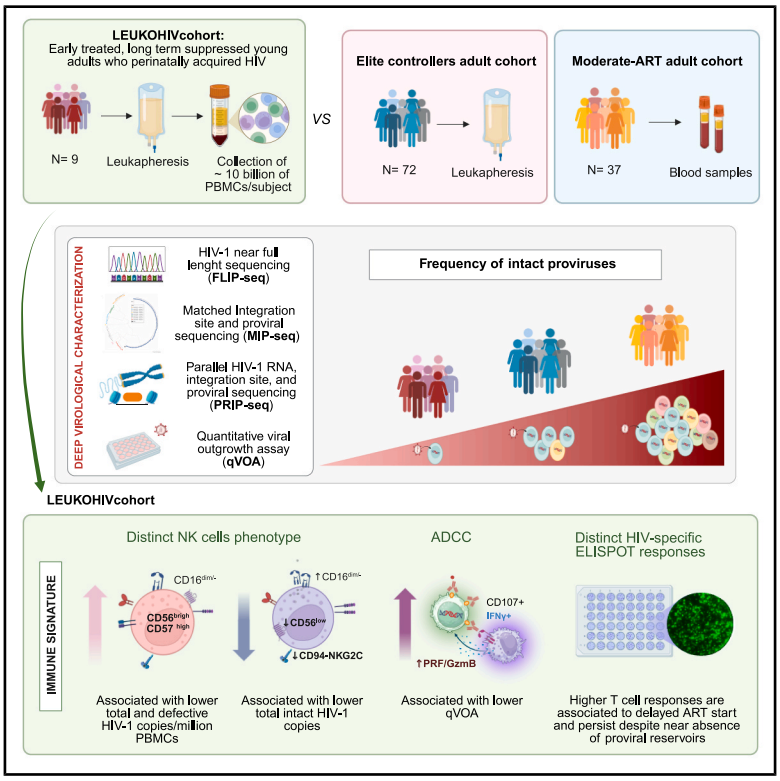

Highlights

- Young adults with perinatally acquired HIV (PHIV) on LT-ART have small viral reservoirs
- In some participants, zero or few intact proviruses were present in a billion PBMCs
- Higher frequencies of CD56^{bright} NK cells observed in PHIV than adults with HIV
- Reservoir size is inversely associated with CD57^{+}CD56^{bright} NK cells and ADCC function

Authors

Benjamin Bone, Nicola Cotugno, Chiara Pighi, ..., Xu G. Yu, Mathias Lichterfeld, Paolo Palma

Correspondence

brb173@med.miami.edu (B.B.), nicola.cotugno@opbg.net (N.C.), mlichterfeld@mgh.harvard.edu (M.L.), paolo.palma@opbg.net (P.P.)

In brief

Bone et al. demonstrate that viral reservoirs of young adults with perinatally acquired HIV, on long-term ART, are exceptionally small and are associated with a distinct phenotypic and functional NK cell signature. This highlights the potential role of innate immune cells in controlling the reservoir that persists during long-term ART.

Bone et al., 2025, Cell Reports Medicine 6, 102150
June 17, 2025
https://doi.org/10.1016/j.xcrm.2025.102150

CellPress

Cell Reports Medicine

CellPress
OPEN ACCESS

Article

Distinct viral reservoirs and immune signatures in individuals on long-term antiretroviral therapy with perinatally acquired HIV-1

Benjamin Bone,[1,2,9,*] Nicola Cotugno,[3,4,9,*] Chiara Pighi,[3] Arianna Rotili,[3,5] Seohyun Hong,[1] Leah Carrere,[1,2] Elena Morrocchi,[3] Giuseppe Rubens Pascucci,[3,4] Ce Gao,[1,2] Nicole Colantoni,[3] Weiwei Sun,[1] Giovanna Leone,[6] David R. Collins,[1] Mpho J. Olatotse,[1] Giovanna Del Principe,[6] Toong Seng Tan,[1] Melanie Lancien,[1] Alessia Neri,[3,5] Libera Sessa,[1,2] Giulio Olivieri,[3,5] Kailey Shapiro,[1] Isabelle Roseto,[1,2] Catherine Koofhethile,[1,2] Elena Emili,[4] Stefania Bernardi,[7] Ann Chahroudi,[8] Paolo Rossi,[4] Bruce D. Walker,[1] Xu G. Yu,[1] Mathias Lichterfeld,[1,2,10,*] and Paolo Palma[3,4,10,11,*]

[1]The Ragon Institute of MGH, MIT and Harvard, Boston, MA, USA
[2]Infectious Disease Division, Brigham Women's Hospital, Boston, MA, USA
[3]Clinical Immunology and Vaccinology Unit, IRCCS, Bambino Gesù Children's Hospital, Rome, Italy
[4]Chair of Paediatrics, Department of Systems Medicine, University of Rome "Tor Vergata", Rome, Italy
[5]PhD Program in Immunology, Molecular Medicine and Applied Biotechnology, University of Rome "Tor Vergata", Rome, Italy
[6]Transfusion Unit, IRCCS, Bambino Gesù Children's Hospital, Rome, Italy
[7]Infectious Diseases Unit, IRCCS, Bambino Gesù Children's Hospital, Rome, Italy
[8]Department of Pediatrics, Emory University School of Medicine, Atlanta, GA, USA
[9]These authors contributed equally
[10]Senior author
[11]Lead contact
*Correspondence: brb173@med.miami.edu (B.B.), nicola.cotugno@opbg.net (N.C.), mlichterfeld@mgh.harvard.edu (M.L.), paolo.palma@opbg.net (P.P.)
https://doi.org/10.1016/j.xcrm.2025.102150

SUMMARY

Early initiation of antiretroviral therapy (ART) following HIV-1 infection restricts the size of the latent reservoir, following both horizontal and vertical infections. Here, we comprehensively profile the reservoirs and immunological milieus of nine young adults who acquired HIV-1 perinatally and remained on suppressive long-term ART (median: 20 years) since infancy (LeukoHIV cohort). Genome-intact reservoirs are markedly smaller compared to a cohort of adults on suppressive ART started in adulthood, with some LeukoHIV individuals characterized by an absence or near absence of intact proviruses in up to a billion peripheral blood mononuclear cells (PBMCs). Higher frequencies of functional CD56^{bright} natural killer (NK) cells with increased cytotoxic activity are detectable in the LeukoHIV cohort compared to an adult reference cohort, while one LeukoHIV participant displayed a potent HIV-1-specific CD8^{+} T cell response. Collectively, our data suggest that long-term ART initiated in early life following perinatal transmission may facilitate an immune environment better equipped to restrict the HIV-1 reservoir.

INTRODUCTION

Despite continuous progress in antiretroviral drug development, HIV-1 infection remains one of the very few infectious diseases for which no curative treatment options are available; life-long suppressive therapy is the only available treatment modality for approximately 39 million people living with HIV-1 (PLWH) worldwide.[1] Lifelong persistence of HIV-1 reservoir cells, necessitating indefinite antiretroviral medication intake, is frequently a particular challenge for children, teenagers, and young adults living with HIV-1, who cumulatively include more than 2.58 million individuals worldwide and whose number is growing by at least 130,000–140,000 new cases each year.[1] Many of these individuals acquired HIV-1 infection pre- or perinatally; in fact, insufficient maternal access to effective preventions for perinatal transmission 10–20 years ago resulted in a generation of teenagers and young adults living with HIV-1 in many sub-Saharan countries today.[2,3] Although suppressive antiretroviral therapy (ART) was frequently started early in such individuals, sometimes within days or weeks after birth, the pharmacological suppression of viral replication in children and young adults is frequently suboptimal.[4–6] Indeed, recent data from the World Health Organization suggest that less than half (46%) of all children living with HIV-1 have reached the therapeutic goal of viral suppression,[7] often due to insufficient treatment adherence that can result from inadequate access to healthcare providers, unstable relationships with primary caregivers, and social difficulties in coping with a chronic viral illness.[8–10] Nevertheless, there is a growing

community of teenagers and young adults with pre-/perinatal HIV-1 acquisition who started ART soon after birth and remained on suppressive treatment for extended periods of time, in some cases, for up to two decades. Reservoir dynamics within these individuals have become a point of interest within the scientific community[11–13] as they offer unique opportunities to investigate the long-term viral HIV-1 persistence in the pediatric immune system and to evaluate how pediatric immune effector cells may interact with, engage, and possibly restrict the HIV-1 reservoir.

In adults with HIV-1, recent studies clearly documented that genome-intact, replication-competent HIV-1 proviruses can persist for more than two decades through proliferation of infected cells[14–16]; however, the exact modalities for the persistence of specific proviruses remain a matter of active investigation.[17] Instead of a gradual decline of the reservoir cell pool during prolonged ART, prior studies highlighted that, with continuous ART for over two decades, HIV-1 reservoir cells can either remain stable, decrease, or expand as a result of clonal proliferation of virally infected cells.[14,16] Moreover, a deeper molecular analysis of viral reservoir cells, including single-cell assessments of their phenotypic, genomic, and epigenetic properties, suggested selective persistence of HIV-1 reservoir cells that are optimally adjusted to host immune activity[18]; in particular, long-term persistence of viral reservoir cells was associated with proviral integration into repressive chromatin compartments[19] and with phenotypic features suggestive of proviral transcriptional repression and resistance to immune-mediated killing.[18,20] Together, these studies suggest that the immune systems of adults, in the setting of horizontally acquired HIV-1, may be able to mount immunological selection pressure against the viral reservoir cell pool, which may facilitate the targeted elimination of at least some of the infected cells.[21] In contrast, very little is currently known about how the pediatric immune system can interact with, and possibly target, HIV-1 reservoir cells during long-term ART.

In this study, we investigated viral reservoir profiles and immunologic effector cell features in a cohort of individuals (LeukoHIV cohort) who acquired HIV-1 perinatally, initiated ART early in life, and remained on suppressive ART for a median of 20 years. Through a detailed virological and immunological analysis of large numbers of cells, we assessed the persisting viral reservoir during continuous ART, relative to a comparison cohort of ART-treated adults. We observed that persisting viral reservoir cells in individuals with perinatal HIV are frequently extremely low and display marked footprints of immune selection.

RESULTS

HIV-1 proviral reservoirs in the LeukoHIV cohort

We performed an analysis of HIV-1 reservoir cells in all study participants of the LeukoHIV cohort, which comprises teenagers and young adults (n = 9, 7 female, 2 male), all of whom acquired HIV-1 infection perinatally and started ART within the first months of life (median: 4 months, interquartile range [IQR]: 3.6–5.8 months); subsequently, they remained on long-term suppressive ART for a median of 20 consecutive years (IQR: 13–22 years). The clinical characteristics of the study cohort are summarized in Table 1. For a deep characterization of the HIV-1 reservoir cell pool, we subjected peripheral blood mononuclear cells (PBMCs) from the study participants to single-genome, near full-length HIV-1 next-generation sequencing (FLIP-seq) and, in some study participants, to matched integration site and proviral sequencing (MIP-seq), using protocols described in our previous work.[22,23] Both of these assays can amplify near full-length HIV-1 proviruses at a single-genome resolution, with subsequent bioinformatical analysis facilitating further assessment to determine whether a given sequence possesses lethal defects or is genome intact. In the nine participants from the LeukoHIV cohort, large numbers of PBMCs collected by leukapheresis were available for investigation, allowing us to study a median of 86 million PBMCs (IQR: 6.2×10^7–9.9×10^8 PBMCs). For comparative analytic purposes, we leveraged prior published data on two cohorts: a cohort of adults treated with ART, with a median of 8 years of undetectable HIV-1 replication (range: 1–14 years), designated the moderate (m)-ART cohort; and a group of elite controllers who maintain undetectable levels of HIV-1 replication in the absence of ART for a median of 9 years (range: 1–24 years) (EC cohort).[24]

Overall, we noted that frequencies of total HIV-1 proviruses from LeukoHIV study participants were significantly lower compared to the m-ART cohort but not different relative to elite controllers (Figure 1A). The frequency of intact HIV-1 proviruses trended lower for the LeukoHIV cohort in comparison to both reference cohorts, although these differences only reached statistical significance when compared to the m-ART cohort (Figure 1B). Of note, in one study participant (LeukoHIV01) from the LeukoHIV cohort, we failed to detect a single intact provirus despite analyzing 1 billion PBMCs; moreover, in one additional study person (LeukoHIV05), only 1 intact provirus was detected after analyzing 990 million PBMCs. The size of the defective reservoirs for the LeukoHIV cohort was also lower compared to the m-ART cohort (Figure 1C), and the proportions of genome-intact proviruses within the total number of proviruses identified in a given study participant were smaller in the LeukoHIV cohort compared to the two reference cohorts (Figure 1D), reflecting the large number of defective sequences detected in most LeukoHIV study participants. Out of those defective proviruses, sequences with large deletions dominated the viral reservoir landscape in the LeukoHIV cohort, with few other defects detected other than hypermutated sequences (Figure 1E). One possible explanation for the low frequency of genome-intact proviruses was that clonal proliferation, known to stabilize and expand the viral reservoir cell pool in adults,[25–27] was reduced in the LeukoHIV cohort. However, analysis of the proportions of sequence-identical, genome-intact clonal sequences in the LeukoHIV cohort failed to demonstrate evidence for a reduced number of clonal genome-intact proviruses in these study persons relative to the EC and m-ART cohorts (Figures 1F and 1G). We propose that the low levels of intact HIV-1 observed in the LeukoHIV study participants are likely a consequence of host immune effects against cells harboring intact HIV-1, which generally seem to be more susceptible to antiviral immune mechanisms compared to cells harboring defective HIV-1 DNA.[16,18,28,29]

Table 1. Clinical characteristics of the LeukoHIV cohort

Pt code	Gender	Age at enrollment (years)	Race	Age at ART start (month)	Co-infection at birth	First type of ART available	Time to HIV suppression (months)	Time on suppressive ART (years)	Occurrence of detectable HIV viral load	Time of last detectable HIV (years)	Anti-CMV_IgG
LeukoHIV01	F	19.2	Black	3.9	none	ZDV + 3TC + LPV/r	2.50	18	none in the last 14 years	none in the last 14 years	positive
LeukoHIV02	F	12	Caucasian	5.13	CMV	ZDV + 3TC + LPV/r + NVP	2.9	11	none	11	positive
LeukoHIV03	F	9.4	Black	4.5	none	ZDV + 3TC + NVP	6	8	none in the last 14 years	none in the last 14 years	negative
LeukoHIV04	F	12	Caucasian	9.2	none	ABC + 3TC + NVP	2.5	11	1 blip	2	negative
LeukoHIV05	M	14.4	Caucasian	0.23	CMV	ZDV + ABC + 3TC + NVP	4	14	none	13	positive
LeukoHIV06	F	20.8	Black	3.7	unknown	ABC + 3TC + LPV/r	10	20	1 blip	2	positive
LeukoHIV07	M	21.2	Caucasian	5.9	none	ABC + 3TC + ZDV	within 12 months	20	none in the last 14 years	none in the last 14 years	positive
LeukoHIV08	F	23.9	Caucasian	3.2	none	ABC + 3TC + ZDV	0.75	23	1 spike	14	negative
LeukoHIV09	F	26.9	Caucasian	5.8	none	ABC + 3TC + EFV	18.25	25	1 rebound, 1 failure	none in the last 14 years	negative

To complement our sequencing measurements of the genome-intact proportion of the viral reservoir for the LeukoHIV cohort, we performed traditional *in vitro* viral outgrowth assays. Due to an absence of outgrowth data for the m-ART cohort, we here compared our data to quantitative viral outgrowth assay (QVOA) data from the EC cohort and a different adult cohort of individuals on long-term ART (median: 20 years; IQR: 13–22 years) (LT-ART cohort). In these experiments, no replication-competent HIV-1 could be isolated from study participants LeukoHIV01 and LeukoHIV05, despite analyzing 300 and 502 million $CD4^+$ T cells isolated from 1.75 billion and 2.3 billion PBMCs, respectively (Figure 1H); this absence of outgrowth in such large quantities of cells is comparable to prior data from the San Francisco and Esperanza patients, who may have reached a virological cure of HIV-1 infection in the absence of ART.[24,31] Moreover, no outgrowth was detected in 430 million $CD4^+$ T cells for LeukoHIV09; this result is concordant with the very low frequency of intact proviruses ($n = 7$ in 1.19×10^9 PBMCs) detected by proviral sequencing in this study person.

To assess viral phylogenetic diversity within the viral reservoirs of each participant, we generated a phylogenetic tree of all genome-intact proviruses detected (Figure 1I), which displayed distinct clustering of sequences from each individual study participant. The number of histocompatibility leukocyte antigen (HLA) class I-adapted mutations and the proportion of cytotoxic T cell (CTL) epitopes (restricted by autologous HLA class I alleles) with wild-type sequences were also assessed using bio-computational methods previously described.[16,30] A reduced number of sequences with HLA class I-adapted mutations, paired with an increased proportion of HIV-1 CTL epitopes with wild-type sequences, were observed in the LeukoHIV study persons relative to the m-ART group (Figures 1J and 1K), indicating a more limited development of viral CTL escape. We finalized our cohort reservoir analyses by assessing whether the timing of ART initiation during early life influenced the viral reservoir, performing linear regressions and Spearman's correlations between reservoir assessments and the timing of ART initiation. While there was a slight trend for a positive correlation between total reservoir size and time of ART initiation after birth, these trends were not significant (Figure 1L).

Collectively, our reservoir analyses of the LeukoHIV cohort revealed remarkably small reservoir sizes within these individuals in comparison to long-term ART-treated adults described here and elsewhere[14,16]; at least in part, these low reservoirs could be due to enhanced immune targeting of cells harboring intact proviruses by the pediatric immune system.

Integration sites of genome-intact proviral sequences in the LeukoHIV cohort

To extend our investigation of HIV-1 reservoir cells, we used MIP-seq to identify the virus-host genome junction and corresponding integration sites for genome-intact proviruses (Figure 2), considering prior work suggesting that proviral positioning in the human genome can be regarded as a biomarker of immune selection occurring within the viral reservoir cell pool.[16,23] In three of the nine LeukoHIV participants (LeukoHIV02, LeukoHIV04, and LeukoHIV06), clusters of sequence-identical intact proviruses

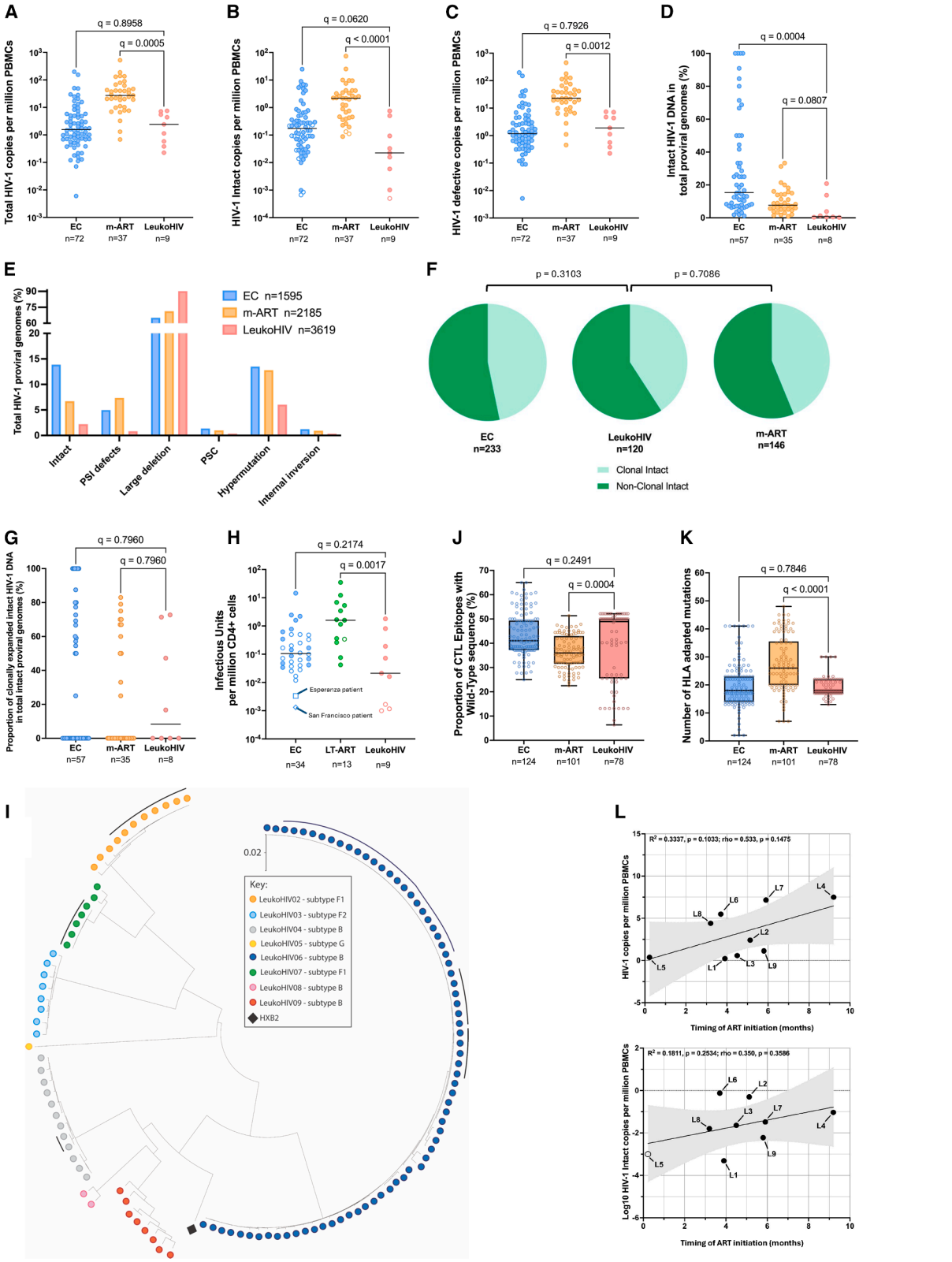

(legend on next page)

were identified by near full-length proviral sequencing; moreover, in one more study participant (LeukoHIV07), a cluster of clonal intact proviruses was observed after near full-genome sequencing of proviruses isolated from viral outgrowth assays conducted with large numbers of cells. No clonal clusters were observed in LeukoHIV03, LeukoHIV08, and LeukoHIV09 (Figure S1); we omitted phylogenetic investigations of LeukoHIV01 and LeukoHIV05 as no intact proviruses were detected for LeukoHIV01 and only a single intact provirus was detected for LeukoHIV05. The very low frequencies of intact proviruses in the majority of the LeukoHIV study participants only permitted the identification of integration sites of intact proviruses in two study participants: LeukoHIV02 and LeukoHIV06. In LeukoHIV02, a large clone integrated in a genic position on chromosome 3 was noted. For LeukoHIV06, the study participant with the highest frequency of genome-intact proviruses in the entire cohort, a total of 72 intact proviruses were detected that could be segregated into multiple clonal clusters of sequence-identical intact proviruses; these clusters of clonal sequences shared considerable sequence similarity to one another, and nucleotide differences between individual clones were frequently limited to one or two base pair residues. Integration site profiling in this study person demonstrated a large clone of genome-intact proviruses integrated into the ZNF718 (ZNF, zinc finger protein) gene, located in the telomeric region of chromosome 4. One additional genome-intact sequence was identified in ZNF721, also in the telomeric region of the chromosome, and one more intact provirus was detected in a ZNF gene on chromosome 19. Notably, using an assay to evaluate the transcriptional behavior of individual proviruses in conjunction with the proviral integration site directly *ex vivo*,[19] we noted that all proviruses integrated in ZNF genes were transcriptionally silent, while a number (n = 15) of genome-defective proviruses that were integrated in genic regions frequently expressed readily detectable viral transcripts (Figures 3A and 3B). These observations support the hypothesis that proviruses in ZNF regions, when assessed directly *ex vivo*, are transcriptionally repressed, likely through concerted epigenetic effects including TRIM28, which facilitates the recruitment of suppressive histone modifications,[32,33] as well as the human silencing hub complex, a notable repressor of endogenous retroviruses and retrotransposons.[34] Three intact proviruses were noted in study person LeukoHIV06 outside of ZNF genes: one in a non-genic region on chromosome 15, which was observed to transcribe viral long-LTR RNA, and two proviruses in genic positions, for which viral transcriptional activity could not be assessed. Together, these data suggest that the integration sites of genome-intact proviruses in study participant LeukoHIV06 are biased toward ZNF genes, findings that draw parallels with EC cohorts and post-treatment controllers.[16,24]

Functional HIV-1-specific T cell response and HIV antibody persistence in the LeukoHIV cohort

Of the nine LeukoHIV cohort members, very low frequencies of intact HIV-1 proviruses were detected by near full-length sequencing for participants LeukoHIV01, LeukoHIV05, and LeukoHIV09. We therefore evaluated their immunological milieus, initially measuring their HIV-1-specific T cell immune responses. T cell production of interleukin (IL)-2 and interferon (IFN)-ɣ following Gag and Env peptide stimulation was monitored, with a strong immune response observed for both IL-2 and IFN-ɣ in LeukoHIV09, a person with delayed ART initiation after birth. In addition, a higher proportion of IL-2-secreting Gag-specific T cells was also observed for LeukoHIV09, LeukoHIV06, and LeukoHIV07 (Figures 4A and 4B).

To further investigate T cell responses against HIV-1 in environments where there is a near absence of intact proviruses, we mapped and functionally profiled $CD8^+$ T cell responses in LeukoHIV01, LeukoHIV05, and LeukoHIV09 against optimal HIV-1 epitopes restricted by autologous HLA isotypes, using IFN-ɣ ELISpot assays and CFSE-based proliferation

Figure 1. HIV-1 proviral reservoir dynamics of the LeukoHIV cohort compared with a cohort of elite controllers and individuals on moderate-term (8 years) suppressive ART

(A–C) Frequency of total HIV-1 copies (A), genome-intact HIV-1 copies (B), and defective HIV-1 copies (C), per million PBMCs assayed, as detected by FLIP/MIP-seq. Open circle data points for cohorts in (B) indicate that the measurement is below the limit of detection.

(D) Proportion of genome-intact HIV-1 copies within the total sequences identified by FLIP/MIP-seq.

(E) Proportion of different sequence types of total HIV-1 sequences detected by FLIP/MIP-seq, including genome-intact, sequences with Psi defects, sequences with large deletions, sequences with premature stop codons (PSCs), hypermutated sequences, and sequences with internal inversions.

(F) Parts of a whole analysis demonstrating proportions of intact sequences that are clonally identical to other sequences, and intact sequences that were detected only once, for each cohort.

(G) Proportions of clonally intact proviruses within the total pool of genome-intact proviruses.

(H) Frequency of replication-competent HIV-1 per million $CD4^+$ cells assayed by quantitative viral outgrowth assay (QVOA). Open circle data points indicate that the measurement is below the limit of detection.

(I) Maximum-likelihood phylogenetic tree of all genome-intact HIV-1 proviral sequences across the LeukoHIV cohort. Each symbol corresponds to an intact provirus detected for each member of the LeukoHIV cohort, with the symbol color relating to the respective study participant, virus clades annotated in key. As no intact sequences were detected for LeukoHIV01, no sequences are shown for that individual. Tree is rooted to a HXB2 (clade B) reference sequence.

(J) The number of base pair variations within individual unique genome-intact proviruses significantly associated with autologous class I HLA alleles, as determined in a prior study.[30] Each symbol represents one provirus. Clonal sequences were counted only once. Box and whisker plots present median, IQRs, and minimum/maximum values.

(K) Proportion of wild-type clade B CTL epitopes restricted by autologous class I HLA alleles from individual unique genome-intact proviruses. Each symbol represents one provirus. Clonal sequences were counted only once. Box and whisker plots present median, IQRs, and minimum/maximum values.

(L) Linear regression of the timing of ART initiation (months) against HIV-1 copies per million PBMCs (left) or $\log_{10}$ transformed genome-intact HIV-1 copies per million PBMCs (right). Regression R^2 and p value presented. Spearman's correlation rho and p value presented. Open circle data points indicate that the measurement is below the limit of detection and gray area represents the confidence interval.

(A, B, C, D, G, H, J, and K) Kruskal-Wallis tests performed with false discovery rate (FDR) adjusted p values (presented as q values). (E) Fisher's exact test performed on contingency table data, these data presented here in pie chart format, p values presented.

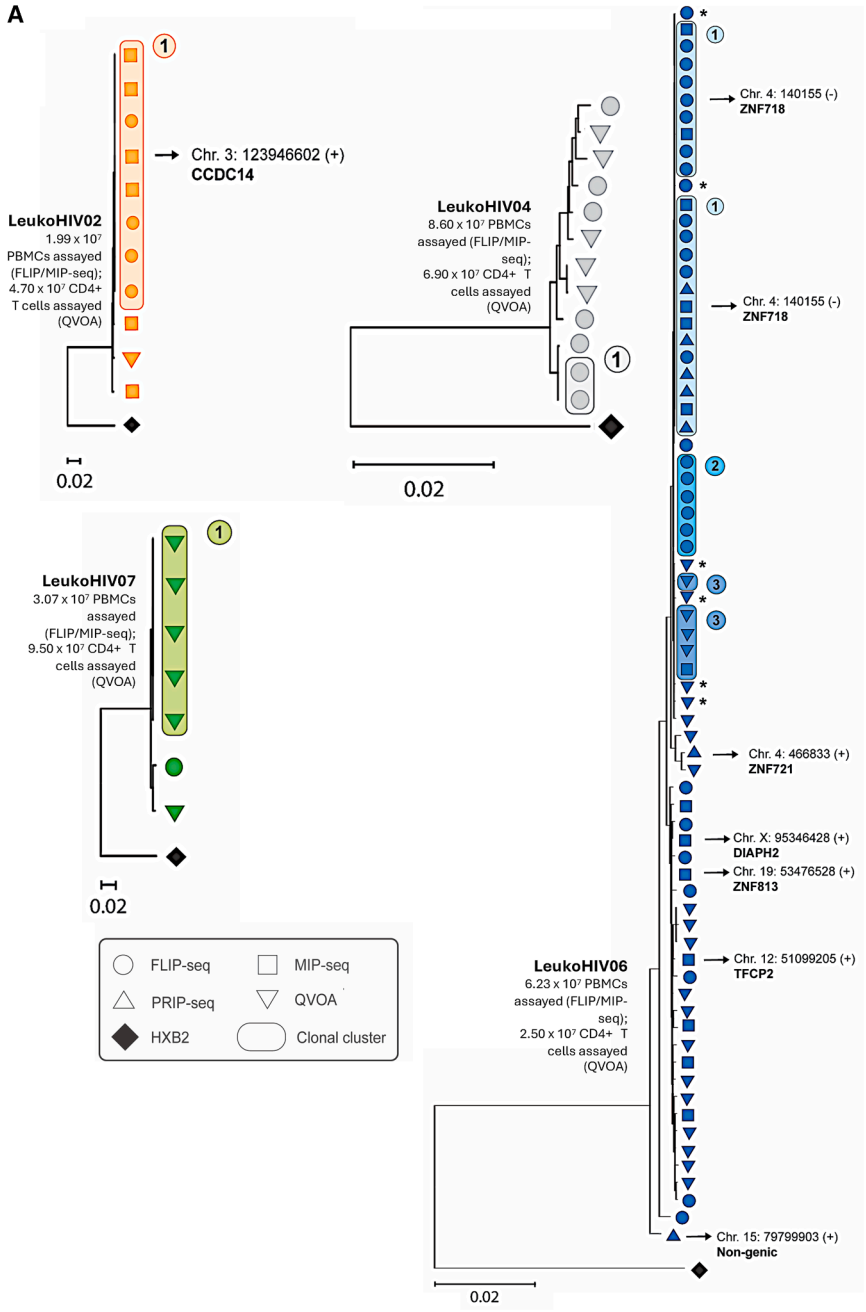

Figure 2. Phylogeny and chromosomal positioning of HIV-1 intact proviruses in participants LeukoHIV02, LeukoHIV04, LeukoHIV06, and LeukoHIV07

(A) Maximum-likelihood phylogenetic trees for HIV-1 intact proviruses detected by near full-length sequencing technologies for LeukoHIV02, LeukoHIV04, LeukoHIV06, and LeukoHIV07. All trees are rooted to an HXB2 reference sequence. Each symbol corresponds to a single intact sequence with the symbol shapes pertaining to the sequencing technology used to detect the respective provirus (see key). Clonal sequences are emphasized through the symbols being encircled, with clonal group numbers annotated. Sequences that differ by 1–2 base pairs from adjacent clonal sequences are labeled with an (*). Specific proviral integration site coordinates generated through MIP-seq are documented on the trees, and the gene name is indicated where applicable. Cells assayed by FLIP/MIP-seq and QVOA are displayed with their respective tree.

assays. No responses were observed in LeukoHIV01 and LeukoHIV05, whereas LeukoHIV09 harbored two non-proliferative subdominant responses against the HLA-B*14-restricted Env EL9 (ERYLKDQQL) and the B*51-restricted Pol LI9 (LPPVVAKEI) epitopes and a dominant proliferative response against the HLA-B*14-restricted Gag epitope DA9 (DRFYKTLRA) (Figure 4C). The latter response was of comparable magnitude to responses previously observed in durable HIV-1 controllers.[35] The DA9 peptide sequence is present in the autologous LeukoHIV09 HIV-1 intact sequences, which demonstrates that the response has not escaped *in vivo*. Moreover, DA9 is reported to be a highly network epitope, indicating that this residue is topologically important for the integrity of the viral protein[36]; therefore, immune escape within the DA9 epitope would likely result in marked viral fitness costs. To further test whether this persisting cellular HIV-1 immune response extends to the humoral immune response, the presence of HIV-1-specific antibodies (Ab) toward 10 HIV-1 antigens was investigated by western blot (WB) assays. The analysis was performed on samples collected in 2017 and 2022 and showed stable longitudinal results. Indeed, three participants (LeukoHIV01, LeukoHIV05, and LeukoHIV07),[37] in line with previous results, demonstrated HIV-1 seronegativity that was unmodified over time (Figure 4D). In contrast, LeukoHIV06 and LeukoHIV02 showed an increase in cumulative HIV-specific Ab (WB score), presumably related to the viral blip observed in 2020 for LeukoHIV06 (Table 1). LeukoHIV09 presented a high WB score of 4.5, likely due to the more advanced age at ART initiation (6 months), the longer time to reach HIV plasma viral load suppression, and the history of virological failure following stable viral control for 14 years.

The association between HIV-1-specific T cell and humoral responses and the time of antigenic exposure was further investigated by correlation analysis with $CD4^+$ HIV-1-specific T cells. Indeed, antigen (Ag)-specific $CD40L^+$ $CD4^+$ T cells within peripheral T follicular helper (pTfh) cells ($CD3^+CD45RO^+CD27^+CXCR5^+$), investigated by flow cytometry after both Env and Gag peptide stimulation, showed a positive association with both WB score (rho = 0.72, p = 0.028; rho = 0.69, p = 0.04, respectively) and

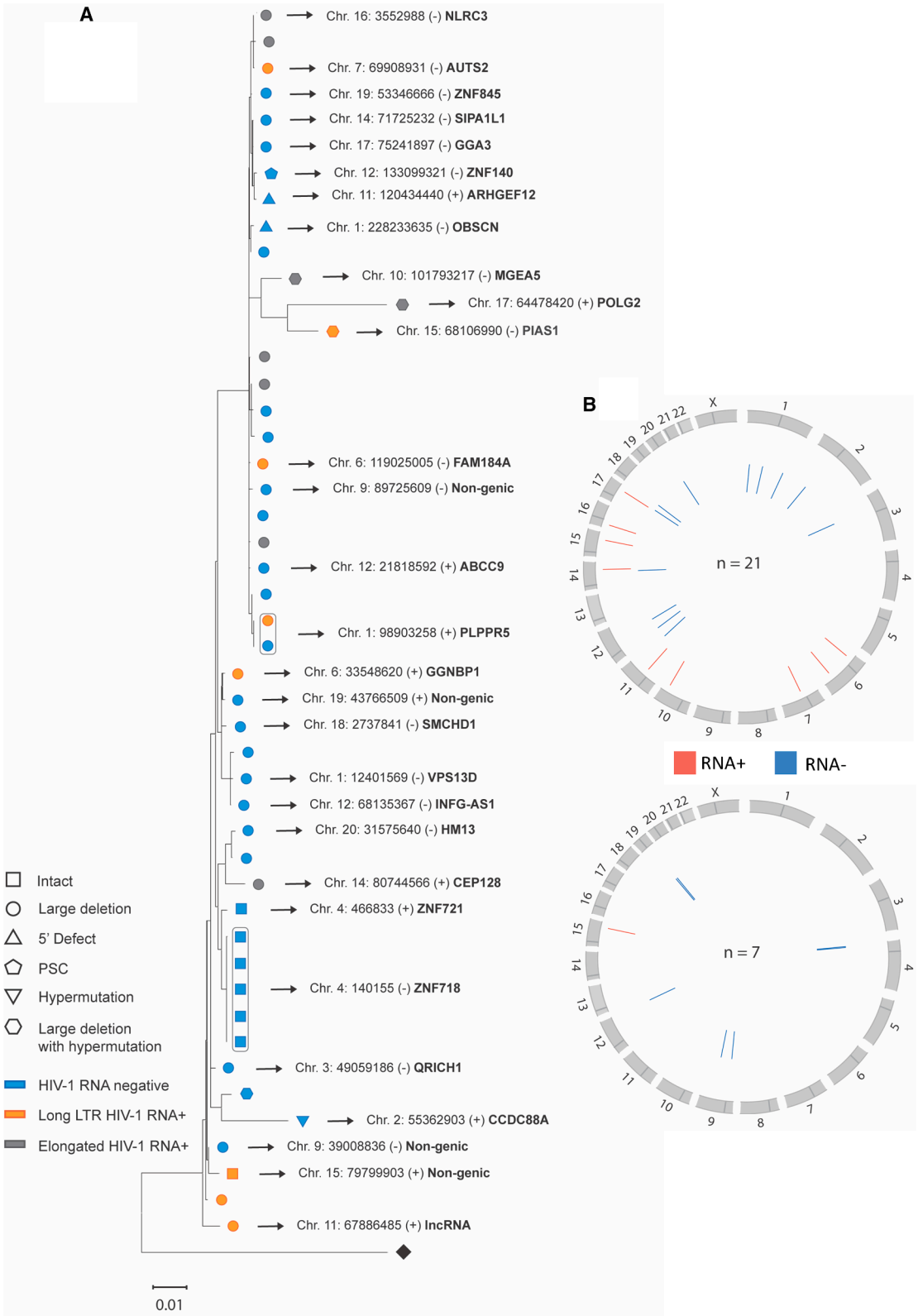

(legend on next page)

with time needed to reach viral load suppression (rho = 0.8; p = 0.009) (Figure 4E).

To complement these results, HIV-1-specific B and T cells and general immune phenotypes were characterized in the LeukoHIV cohort and revealed no major differences among the persons enrolled in terms of distribution of cell subsets (Figures S2, S3A, and S3B). Overall, Ag-specific responses were higher for Gag compared to Env in both total CD4$^+$ T cells and pTfh cells. In particular, a few participants, including LeukoHIV09, LeukoHIV07, LeukoHIV08, and LeukoHIV03, showed a higher frequency of Gag-specific T cells. This was not the case for Env-specific responses where only LeukoHIV09 presented a mild increase compared to the unstimulated condition (Figures S3C and S3D). For the B cell counterpart, gp140$^+$ B cells were investigated in the entire cohort in CD19$^+$IgD$^-$ B cells, in CD27$^+$IgD$^-$CD27$^+$ switched memory B cells, as well as within total IgG$^+$ and IgM$^+$ B cells. LeukoHIV06 presented the highest frequency of Ag-specific B cells compared to the other participants. This result is in line with the increase in HIV Ab WB score (4.5 in 2022 as compared to 3 in 2017), which may suggest a recent viral exposure due to low adherence. However, these data were not confirmed in LeukoHIV09, who had a stable HIV Ab WB over time but no history of viral blips, virological failure, or evidence of integrated intact provirus.

Natural killer cell phenotype and Ab-dependent cellular cytotoxicity against HIV-infected cells in LeukoHIV participants

Acknowledging the ability of natural killer (NK) cells to modulate T cell and antibody responses[38] as well as their crucial role in controlling HIV infection through antibody-dependent cellular cytotoxicity (ADCC), which has been demonstrated in studies highlighting ADCC effects on vaccine-induced protection, viral control, and slowing HIV disease progression,[39–43] we evaluated the NK cell phenotype in LeukoHIV participants and its association with viral reservoir measurements. We assessed the NK cell phenotype (gating strategy reported in Figure S4) as well as markers of NK cell maturation and activation such as CD57, NKG2C, NKp46, DNAM-1, perforin, and granzyme B across distinct subsets of NK cells and compared it to that of an age-matched cohort of participants without HIV. Whereas no major differences emerged among the participants in terms of total NK cell frequency and CD56 expression (Figures S5A and S5B), a wide variability was observed in CD57$^+$NKG2C$^+$CD56^{dim} cells due to cytomegalovirus (CMV) exposure or infection (Table 1), which is known to shape the NK cell repertoire by preferentially expanding a memory-like or adaptive NK cell population co-expressing NKG2C and CD57, displaying a terminally differentiated phenotype with hallmarks of adaptive immunity including clonal expansion, increased longevity, enhanced effector functions, and epigenetic modifications.[44–50] Indeed, LeukoHIV08, LeukoHIV09, LeukoHIV03, and LeukoHIV04, who were IgG negative for CMV, showed the lowest frequency of CD57$^+$NKG2C$^+$CD56^{dim} cells in comparison to the CMV$^-$ seropositive study persons LeukoHIV05, LeukoHIV02, and LeukoHIV06. Indeed, LeukoHIV05 and LeukoHIV02 had a documented history of perinatal CMV co-infection, and there was a high index of clinical suspicion for perinatal CMV infection in LeukoHIV06, although clinical records from this time period for this study participant were not available (Figure S5C). The higher frequency of NKG2C$^+$ cells in these three persons was further confirmed in total NK cells and CD56^{dim} NK cells (Figure S5D).

Compared to an age-matched cohort of participants without HIV, the LeukoHIV cohort exhibited a significantly lower frequency of NK cells, a higher frequency of CD56^{low} cells, and reduced frequencies of CD57$^-$NKG2C$^-$ CD56^{dim} cells, NKp46$^+$ NK cells, or CD56^{bright} or CD56^{dim} or CD56^{low} cells, as well as a lower frequency of CD57$^+$ CD56^{low} cells (Figures S5A–S5D).

To test the ADCC, we performed infected cell elimination assays against the HIV-1-infected 8E5/LAV cell line, using p24 Ag reduction as an outcome parameter.[51,52] In all study participants, we observed the highest killing activity when co-stimulating cells with heterologous hyperimmune plasma compared to either autologous or healthy control plasma (Figure S5E). LeukoHIV05, in line with being HIV seronegative, showed the largest variability between autologous and heterologous plasma suggesting preserved Ab-dependent cellular cytotoxic function upon heterologous induction. LeukoHIV09 (WB score of 4.5) showed the highest killing activity among the cohort when co-stimulated with autologous plasma; this was further confirmed by assays with heterologous plasma stimulation.

To characterize NK-cell mediated ADCC, we investigated the surface mobilization of CD107a upon HIV antibody stimulation along with the expression of CD57, NKG2C, NKp46, DNAM-1, perforin, and granzyme B in degranulating CD107a+ NK cells. In line with a functional p24 reduction, a higher cytotoxic activity was found in LeukoHIV05, LeukoHIV06, LeukoHIV08, and LeukoHIV09 when stimulated with heterologous plasma. Such higher cytotoxic function was further confirmed with autologous plasma (Figure S5F).

NK cell degranulation and its ligands are associated with the composition of the HIV reservoir decades after viral control

To further confirm the unique characteristics of the LeukoHIV cohort, especially within the NK cell phenotype, we identified six NK cell subsets by CD56 and CD16 expression as previously reported[53] (gating strategy in Figure 5A top left panel). We further compared the frequencies of these subsets with those of adult participants living with HIV-1. Such analysis showed a distinct distribution between the subsets among LeukoHIV study participants with a significantly higher frequency of CD56^{bright} CD16^{low}

Figure 3. Transcriptional behaviors of HIV-1 proviruses isolated by PRIP-seq in study participant LeukoHIV06

(A) Maximum-likelihood phylogenetic tree for individual proviruses obtained by PRIP-seq. Symbols indicate the fitness of the corresponding provirus, with the symbol color reflecting the degree of transcriptional activity observed. Chromosomal integration site coordinates and their respective gene locations are annotated on the trees. PSC, premature stop codon.

(B) Circos plot representations of the locations, within the human genome, of HIV-1 transcriptionally expressed (RNA+: red) and inactive (RNA−: blue) proviruses for genic and non-genic DNA.

CellPress
OPEN ACCESS

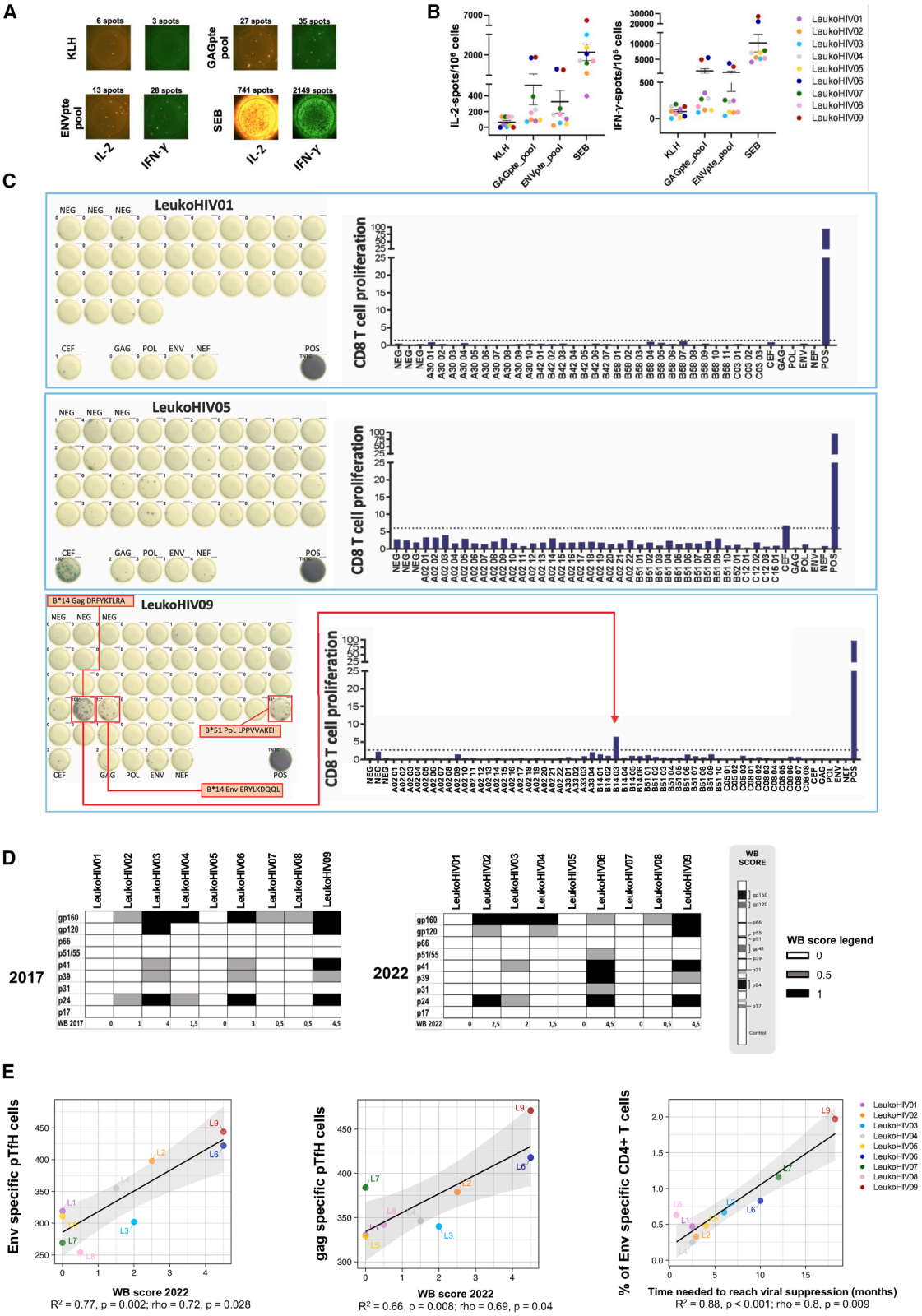

(legend on next page)

(subset III) NK cells (p = 0.029) and lower frequency of both $CD56^{dim}$ $CD16^{-}$ NK cells (subset I) and $CD56^{-}CD16^{+}$ cells (subset V) (p values 0.0053 and 0.0056, respectively) (Figure 5A).

We further interrogated our virological data for possible associations with phenotypic and functional NK cell subsets. Total HIV-1 proviral copies per million PBMCs as well as defective HIV-1 proviral copies per million PBMCs showed a strong negative correlation with $CD57^{+}$ $CD56^{bright}$ NK cells (rho = 0.93 and p value <0.001 for both) (Figure 5B left and middle panels). On the other hand, intact HIV proviral copies per million PBMCs displayed a positive association with the expression of NKG2C within $CD56^{low}$ NK cells (p = 0.02 in Figure 5B right panel).

To further explore the association between HIV-1 viral reservoir analysis and NK cell function, ADCC activity along with surface marker expression was correlated with the distribution of the viral reservoir and QVOA results. Infectious units per million (IUPM) $CD4^{+}$ T cells were negatively associated with $perforin^{+}$ granzyme B^{+} $CD107^{+}$ $IFN\gamma^{+}$ NK cells after autologous plasma *in vitro* stimulation (Figure 5C left panel). Furthermore, both IUPM $CD4^{+}$ T cells and intact HIV-1 copies per million PBMCs were negatively associated with the expression of the NK cell-activating receptor p46 in $CD107a^{-}$ $IFN\text{-}\gamma^{+}$ cells after *in vitro* stimulation with autologous plasma (Figure 5C middle and right panels). For these associations, considering the low variability and extremely low levels for both IUPM and intact HIV-1 copies found in the LeukoHIV cohort, the results from LeukoHIV09, LeukoHIV06, and LeukoHIV07 were the most informative data.

Overall, these analyses further strengthen the hypothesis that a more functional NK cell phenotype persists several years after early ART start in children who perinatally acquired the infection compared to participants who acquired the infection during adulthood.

DISCUSSION

It is well established that the timing of ART initiation has a role in modulating HIV-1 persistence, with distinctly small reservoir sizes (especially within the replication-competent compartment of the reservoir) found in adults who initiated ART early following HIV-1 acquisition.[54,55] The timing of ART initiation is also important in the context of perinatal HIV acquisition, with early treatment affecting reservoir establishment and even leading to cases of sustained aviraemia and spontaneous post-treatment control.[56–58] However, questions remain regarding how this early ART supports the pediatric immune system in perturbing reservoir formation. Here, we sought answers from the unique LeukoHIV cohort participants who are living with perinatal HIV-1 and underwent virological and immunological analyses following a median of 20 years of continuous suppressive ART. Comprehensive reservoir profiling of this cohort demonstrated smaller HIV-1 proviral reservoirs when compared to a cohort of adults on ART. We found distinctively lower frequencies of genome-intact proviruses in LeukoHIV participants and uncovered evidence for potent immune selection pressure in some study participants.

Interestingly, there were three individuals for whom an enrichment of clonally expanded genome-intact sequences was observed: LeukoHIV02, LeukoHIV06, and LeukoHIV07. Previous reports on the integration site patterns of intact proviruses have demonstrated proviral persistence, despite suppressive ART, when the intact proviruses in question were integrated into repressive chromatin regions, such as gene deserts, centromeric/telomeric regions, and ZNF genes[23]; these regions offer protection against immune selection pressure through imposing proviral transcriptional quiescence.[59,60] LeukoHIV06 presented similar integration site patterns, with a bias toward ZNF genes, especially ZNF718 and ZNF721; the latter being a Krab-ZNF gene recently shown to restrict proviral gene expression by up to 200-fold.[61,62] Indeed, our own transcriptomic analysis of LeukoHIV06's genome-intact proviruses indicated minimal transcriptional activity of intact proviruses integrated in ZNF genes, concordant with published literature.[19]

In contrast to LeukoHIV02 and LeukoHIV06, the genome-intact reservoirs of other study participants were more limited. Of note, LeukoHIV01, LeukoHIV05, and LeukoHIV09 were found to have the smallest reservoirs, characterized by an absence or near absence of proviruses and a failure to induce outgrowth by QVOA. Despite similar reservoir features, the immune profile was profoundly distinct among these three individuals. HIV-1-specific $CD8^{+}$ T cell proliferative and IFN-γ responses, against HIV-1 optimal epitopes, were observed for LeukoHIV09, as were strong IL-2- and IFN-γ-secreting T cell responses against HIV-1 peptide pools. Protracted maintenance of HIV-1-specific $CD8^{+}$ T cell responses under ART, such as seen here, has been previously reported although typically in association with

Figure 4. HIV-specific immune responses of the LeukoHIV cohort

(A) IFN-γ/IL-2 FluoroSpot T assay on a representative LeukoHIV subject.

(B) Scatterplots with bar (mean ± SEM) depict IL-2 (Cy3/red) or IFN-γ (FITC, green) spot-forming cells (SFCs) per 10^6 peripheral blood mononuclear cells (PBMCs) after 24-h *in vitro* stimulation of thawed PBMCs, isolated from the LeukoHIV cohort, with HIV Gag or Env peptide pools, keyhole limpet hemocyanin (KLH, negative control), or staphylococcal enterotoxin B (SEB, positive control) on anti-IFN-γ and IL-2-coated plate.

(C) HIV-specific $CD8^{+}$ T cell responses in participants of focus. ELISPOT plates and the subsequent spot counts reflect the IFN-γ secretion in response to HLA-optimal HIV peptides or control treatments. CFSE dilution was used to measure $CD8^{+}$ T cell proliferation (%CFSE-low), highlighting observed responses among 53 total peptides screened. LeukoHIV09 responses were recorded in response to HLA-B*14-restricted Gag epitope DA9 (DRFYKTLRA), HLA-B*14-restricted Env epitope (ERYLKDQQL), and HLA-B*51-restricted Pol epitope (LPPVVAKEI); these are outlined in red, the proliferative response annotated.

(D) Western blot (WB) score tabulated findings for the LeukoHIV cohort. Plasma samples collected in 2017 (left) and 2022 (right) were tested for antibodies against 9 different HIV-1 viral proteins (gp160, gp120, p66, p55/p51, gp41, p39, p31, p24, and p17). The band intensity for each viral antigen was calculated using the ImageJ software. A WB score was assigned to each participant by adding up the number of positive (1, black) and weak (0.5, gray) responses (from 0 to 9).

(E) Scatterplots for WB score (2022) against Env-specific peripheral T follicular helper (pTfh) cell frequency (%) (left), Gag-specific pTfh cell frequency (%) (middle), as well as of Env-specific $CD4^{+}$ T cell frequency (%) against the time needed to reach viral suppression in months (right), with linear regression and correlation analyses performed. Linear regression R^2 and p values presented. Spearman's correlation rho and p values presented. Gray area represents the confidence interval.

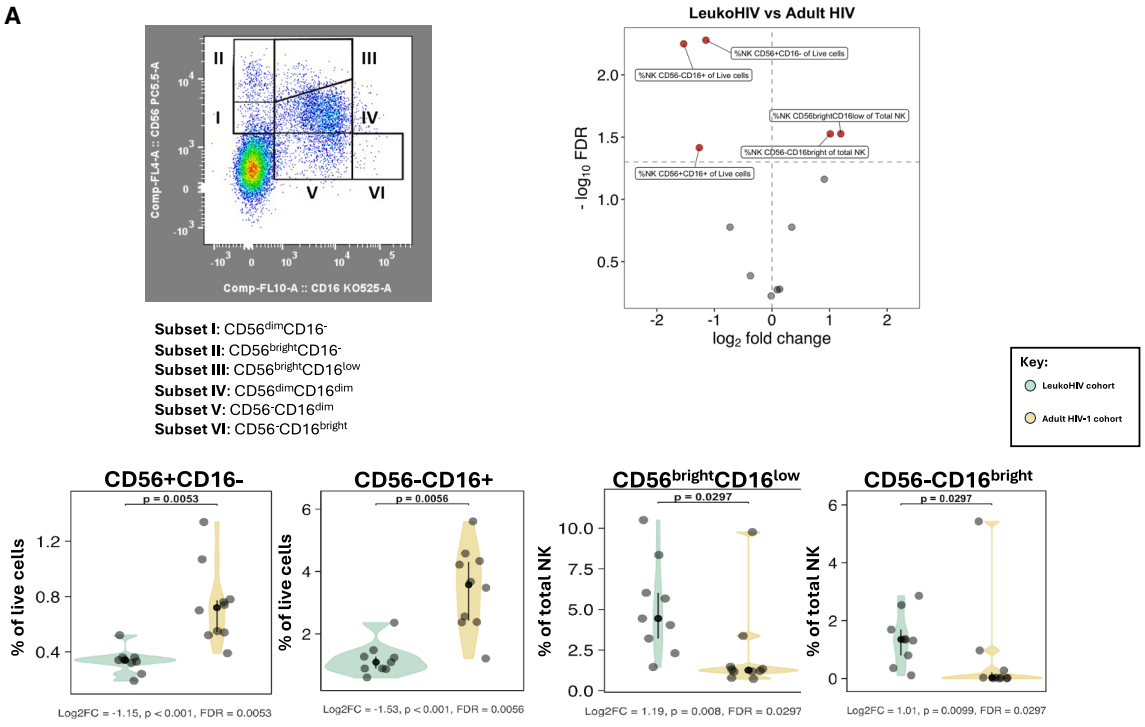

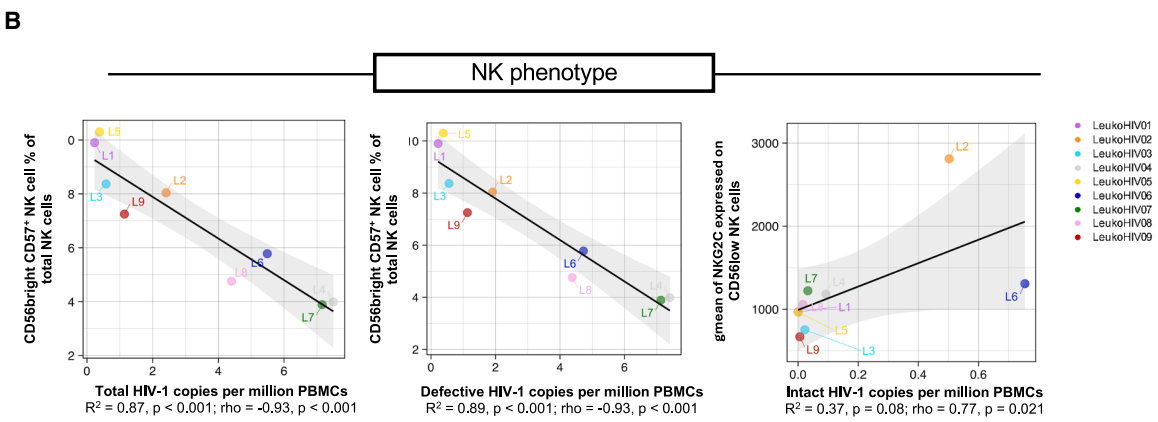

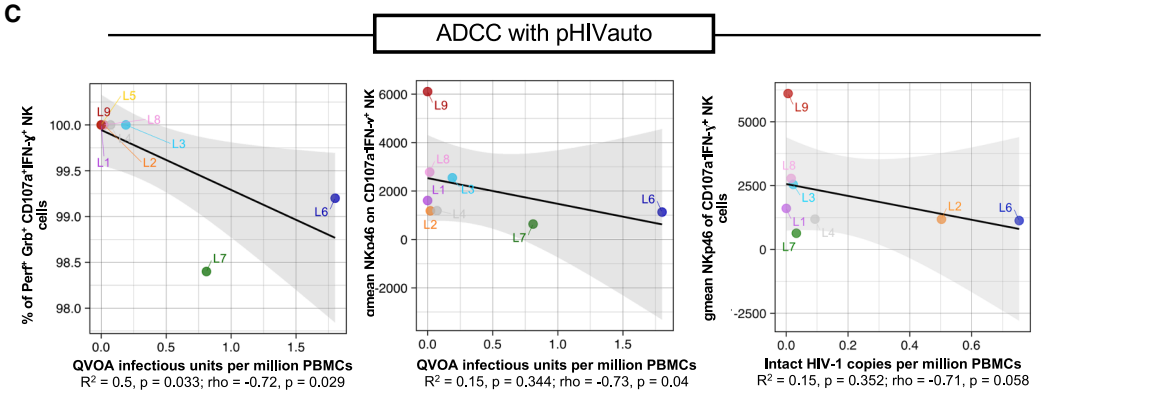

(legend on next page)

high HIV-1 DNA levels.[63,64] Interestingly, LeukoHIV09 was one of the latest cohort participants to start ART at 5.8 months following birth. Considering the critical nature of treatment timing, prolonged exposure to HIV-1 post birth may induce and maintain a persistent memory response, as seen with LeukoHIV09. This is supported by initial immunological data from untreated infants who acquired HIV-1 perinatally, typically exhibiting an HIV-1-specific T cell response after 6 months of age.[65] This delay in treatment initiation for LeukoHIV09, along with a longer time to reach HIV-1 suppression after ART start (18 months) and history of a treatment failure, may have promoted the formation of a heightened $CD8^+$ T memory cell response.[66]

We further explored the immunological behavior of this cohort by examining the NK cell compartment with a specific focus on NK cell function. In line with the enhanced T cell responses observed in LeukoHIV09, NK cell killing activity was the most potent in this individual within the cohort, with elevated NK cell cytotoxic activities also observed in LeukoHIV05, LeukoHIV06, and LeukoHIV08. These results reflect antibody-mediated cytotoxicity; however, it is important to note that NK cell-mediated killing of latently infected cells can occur independently of Ab, a factor not assessed in this study. Correlative assessments between the immunological characteristics of the cohort and reservoir composition demonstrated an inverse relationship between $CD57^+CD56^{bright}$ NK cells and the total reservoir size. Abundance of this NK cell subset as well as their significant cytotoxic function is associated with melanoma patient survival.[67,68] Our results further showed how early-life initiation of ART is able to maintain $CD56^{bright}$ NK cells, which are sequentially found over the acute phase of HIV infection in adult persons.[69,70] Inverse relationships were also observed between infectious units of viral outgrowth and granule effector-expressing NK cells. In addition, the activating receptor-induced expression of NKp46 in degranulating and IFN-ɣ-producing NK cells was inversely related to both intact HIV-1 and QVOA suggesting that the HIV-1 seeding of intact and replication-competent proviruses could be impacted by this unusual NK cell functional activity. Such results confirmed previous findings in elite controllers by comparing these NK cells and total HIV-1 DNA[71] but also highlight the persistence of a distinct NK phenotype of adolescents and young adults living with HIV compared to HIV-negative controls despite early treatment initiation and long-term viral control. This was mainly informed by the significantly higher frequency of $CD56^{low}$ NK and lower NKp46 NK cells found in LeukoHIV participants compared to healthy controls.

An additional finding was the positive association observed between $CD56^{low}$NKG2C, an NK cell-activating factor with "adaptive features,"[47] and intact HIV proviruses. This association, which could be in part driven by the history of CMV infection, confirmed previous results showing the expansion of such subset in the acute phase of HIV infection in adults.[72] Given the high prevalence of CMV seropositivity among PLWH (>90%), the significant skewing and adaptation of the NK cell repertoire following HIV-1 infection are likely influenced by co-infection with CMV.[73] In fact, changes in NKG2C expression on NK cells in PLWH are more closely associated with CMV co-infection rather than HIV-1 infection alone, as including CMV serological status in a multivariate regression model eliminates the positive correlation between elevated levels of $NKG2C^+$ NK cells and HIV-1 infection.

While our data may inform future studies of HIV-1 persistence following early-life ART initiation study, we cannot make absolute statements about the size of the reservoirs of our cohort members. For LeukoHIV01, while we were unable to detect genome-intact HIV-1 proviruses, we by no means draw the conclusion that this individual has eliminated all intact HIV-1 from their body and achieved a "virological cure" status. Such definitive conclusions cannot be made using currently available assays, and a "cure" status can only be designated if no recrudescence is observed following treatment discontinuation. Furthermore, our assessments were based on the peripheral blood compartment of the total HIV-1 reservoir, with substantial evidence indicating that resident $CD4^+$ T cells and myeloid cells in less-studied tissues such as the lymph nodes, gut, and CNS represent a significant proportion of the reservoir, providing challenges for accurate total reservoir measurement.[74] Another caveat to our study lies with the gender balance of the cohort, with a greater representation of females seen compared to males. Female immune systems are characterized by a more potent innate immune response, which may contribute to the reservoir profiles seen. That being said, of the three individuals we selected as having the smallest reservoirs, one was male, indicating that gender may not be a strong influencing factor in our data. The contribution of gender differences should be further investigated especially considering the recent finding of 5 atypical male children maintaining sustained aviraemia in the absence of ART.[56]

Taken together, our data suggest that early ART initiation followed by over a decade of treatment is effective in significantly reducing the HIV-1 viral reservoir and, in some circumstances, to undetectable levels. These viral reservoirs may be the evolutionary product of sustained exposure to unique immune environments. Indeed, for one individual with an expanded genome-intact reservoir, there is evidence of integration of intact proviruses into regions conferring deep latency and shielding from immune detection. For other participants with smaller reservoirs, we observed greater frequencies of cytotoxic NK cells. Pre-analytical treatment interruption (ATI) NK cell responses have been implicated in post-treatment control, with robust responses observed in both the VISCONTI[75] and (AIDS Clinical Trials Group) ACTG cohorts.[76] Furthermore, competent NK cell

Figure 5. Correlation analysis between virological data and NK cells reveals possible associations decades after virological controls

(A) The differential analysis of six distinct NK cell subsets, identified according to the expression of CD56 and CD16 (gating strategy in upper left). Volcano plot in upper right shows the only 5 significantly different NK cell subsets when compared to a cohort of adult participants living with HIV. Differences are also presented as violin plots with Mann-Whitney U tests performed, *p* values presented. Correlation plots for the association between HIV-1 viral reservoir and (B) NK cell phenotype or (C) ADCC analysis upon stimulation with heat-inactivated autologous HIV-1-infected plasma (pHIVauto). Regression R2 and *p* value presented. Spearman's correlation rho and *p* value presented.

responses are involved in the immune control of HIV in neonates,[77] with similar reservoir profiles in infants and the LeukoHIV cohort that correlate with abundant NK cells characterized by a cytotoxic effector phenotype.[53] Further research on how to elicit the favorable immune profiles associated with small/undetectable reservoirs may provide promise to the many young people currently living with HIV-1.

Limitations of the study

With the present study, we cannot make definitive statements about the size of the viral reservoirs of our cohort members, and a "cure" status can only be designated if no recrudescence is observed following treatment discontinuation. Furthermore, our assessments were based on the peripheral blood compartment of the total HIV-1 reservoir, with substantial evidence indicating that $CD4^+$ T cells and myeloid cells residing in less-studied tissues such as the lymph nodes, gut, and CNS represent a significant proportion of the reservoir, providing challenges for accurate total reservoir measurement. Another caveat to our study refers to the gender balance of the cohort, with a greater representation of females seen compared to males. Female immune systems are characterized by a more potent innate immune response, which may contribute to the reservoir profiles reported here.

RESOURCE AVAILABILITY

Lead contact

Further information and requests for resources and reagents should be directed to and will be fulfilled by the lead contact, Paolo Palma (paolo.palma@opbg.net).

Material availability

This study did not generate new unique reagents.

Data and code availability

- Proviral sequencing analysis (FLIP-seq, MIP-seq, and parallel RNA, integration sites, and proviral sequencing [PRIP-seq]): due to participant confidentiality concerns, viral sequencing data cannot be publicly released but will be made available to investigators upon reasonable request to the lead contact and after signing a data sharing agreement.
- This paper does not report custom code.
- Any additional information required to reanalyze the data reported in this paper is available from the lead contact upon request.

ACKNOWLEDGMENTS

We would like to acknowledge study participants and legal guardians. We acknowledge Dr. Chiara Medri for sample processing and Ilaria Pepponi, Jennifer Faudella, and Robert Indaco for administrative assistance.

This work was supported by federal funds from the NIH through the Pediatric Adolescent Virus Elimination Martin Delaney Collaboratory Project Number 1UM1 AI164566-01 (https://www.pave-collaboratory.org/, accessed on January 30, 2023).

This work was also initially supported by EPIICAL (Early-treated Perinatally HIV-infected Individuals: Improving Children's Actual Life with Novel Immunotherapeutic Strategies) project, funded through an independent grant by ViiV Healthcare UK Limited. M. Lichterfeld is supported by NIH grants AI155233, AI152979, AI184094, and AI176579 and by the Bill and Melinda Gates Foundation (INV-002703).

AUTHOR CONTRIBUTIONS

Clinical core activities, leukapheresis, sample processing, and data acquisition, G.L., S.B., N. Cotugno, N. Colantoni, and G.D.P.; FLIP-seq and analysis, B.B., S.H., L.C., L.S., M. Lancien, I.R., K.S., and C.K.; MIP-seq, ISLA, and integration site analysis, B.B., S.H., L.C., L.S., and I.R.; PRIP-seq and analysis, W. S. and B.B.; QVOA and analysis, B.B.; comparative reservoir analyses, B.B. and T.S.T.; bioinformatical processing and analyses, C.G. and G.R.P.; HIV-specific $CD8^+$ T cell response assessment and analysis, D.R.C., M.J.O., G. O., A.N., and B.D.W.; NK, T, and B cell phenotype and functional analysis, C.P., E.M., A.R., A.N., and G.O.; collective data analysis, interpretation, and presentation, B.B., N.C., G.R.P., C.G., X.G.Y., M. Lichterfeld, and P.P.; manuscript preparation, B.B., N. Cotugno, M. Lichterfeld, and P.P.; research project consultation, A.C. and P.R.; research idea, concept, and study supervision, N. Cotugno, P.P., and M. Lichterfeld; funding acquisition, N. Cotugno, P.P., and M. Lichterfeld.

DECLARATION OF INTERESTS

N. Cotugno, P.P., and G.R.P. are respectively CEO and co-founders at Probiomics SRL.

STAR★METHODS

Detailed methods are provided in the online version of this paper and include the following:

- KEY RESOURCES TABLE
- EXPERIMENTAL MODEL AND STUDY PARTICIPANT DETAILS
  - LeukoHIV cohort
  - Cell lines
- METHOD DETAILS
  - Leukapheresis
  - DNA extraction
  - Reservoir quantification estimation
  - HIV-1 near full-length amplification and sequencing
  - Integration site analysis
  - Analysis of transcriptional behavior of HIV-1 proviruses
  - *In vitro* quantification of the replication competent reservoir
  - IFN-γ/IL-2 FluoroSpot T cell assays
  - HIV-1 epitope-specific $CD8^+$ T cell response mapping by IFN-γ elispot
  - HIV-1 epitope-specific CD8 T cell proliferation assay
  - HIV Ab western blot
  - Ag specific T and B cell detection by flow cytometry
  - NK cell immunophenotyping
  - Antibody-dependent cellular cytotoxicity (ADCC)
  - Infected cell elimination assays
  - High-dimensional analysis of flow cytometry data (tSNE and FlowSOM)
- QUANTIFICATION AND STATISTICAL ANALYSIS

SUPPLEMENTAL INFORMATION

Supplemental information can be found online at https://doi.org/10.1016/j.xcrm.2025.102150.

Received: October 14, 2024
Revised: January 31, 2025
Accepted: May 1, 2025
Published: May 29, 2025

REFERENCES

1. HIV/AIDS GJUNPo. UNAIDS Data 2023. 2023.

2. Chi, B.H., Adler, M.R., Bolu, O., Mbori-Ngacha, D., Ekouevi, D.K., Gieselman, A., Chipato, T., Luo, C., Phelps, B.R., McClure, C., et al. (2012). Progress, Challenges, and New Opportunities for the Prevention of Mother-to-Child Transmission of HIV Under the US President's Emergency Plan for AIDS Relief. J. Acquir. Immune Defic. Syndr. *60*, S78–S87.

3. UNAIDS/WHO. Epidermiological fact sheets on HIV/AIDS and Sexually Transmitted Infections, 2004 Update. 2004.

4. Boerma, R.S., Boender, T.S., Bussink, A.P., Calis, J.C.J., Bertagnolio, S., Rinke de Wit, T.F., Boele van Hensbroek, M., and Sigaloff, K.C.E. (2016). Suboptimal Viral Suppression Rates Among HIV-Infected Children in Low- and Middle-Income Countries: A Meta-analysis. Clin. Infect. Dis. *63*, 1645–1654.

5. Han, W.M., Law, M.G., Egger, M., Wools-Kaloustian, K., Moore, R., McGowan, C., Kumarasamy, N., Desmonde, S., Edmonds, A., Davies, M.A., et al. (2021). Global estimates of viral suppression in children and adolescents and adults on antiretroviral therapy adjusted for missing viral load measurements: a multiregional, retrospective cohort study in 31 countries. Lancet. HIV *8*, e766–e775.

6. Tagarro, A., Domínguez-Rodríguez, S., Cotton, M., Otwombe, K., Klein, N., Lain, M.G., Nhampossa, T., Maiga, A.I., Barnabas, S., Vaz, P., et al. (2024). High mortality following early initiation of antiretroviral therapy in infants living with HIV from three African countries. eClinicalMedicine *73*, 102648.

7. UN/WHO. New WHO Guidance on HIV Viral Suppression and Scientific Updates Released at IAS 2023 2023 [Available from: https://www.who.int/news/item/23-07-2023-new-who-guidance-on-hiv-viral-suppression-and-scientific-updates-released-at-ias-2023.

8. Mengesha, M.M., Embibel, M., Gobena, T., Tunje, A., Jerene, D., and Hallström, I.K. (2022). Antiretroviral therapy non-adherence among children living with HIV in Dire Dawa, Eastern Ethiopia: a case-control study. BMC Pediatr. *22*, 653.

9. Fetzer, B.C., Mupenda, B., Lusiama, J., Kitetele, F., Golin, C., and Behets, F. (2011). Barriers to and facilitators of adherence to pediatric antiretroviral therapy in a sub-Saharan setting: insights from a qualitative study. AIDS Patient Care STDS *25*, 611–621.

10. Alemayehu, B., Etana, B., and Abebe, M. (2023). Adherence to Antiretroviral Therapy and Associated Factors Among Children Living With HIV in East Wallaga Zone Public Health Institutions, Ethiopia. J. Int. Assoc. Provid. AIDS Care *22*, 23259582231215677.

11. Uprety, P., Patel, K., Karalius, B., Ziemniak, C., Chen, Y.H., Brummel, S.S., Siminski, S., Van Dyke, R.B., Seage, G.R., and Persaud, D.; Pediatric HIV/AIDS Cohort Study PHACS (2017). Human Immunodeficiency Virus Type 1 DNA Decay Dynamics With Early, Long-term Virologic Control of Perinatal Infection. Clin. Infect. Dis. *64*, 1471–1478.

12. Uprety, P., Chadwick, E.G., Rainwater-Lovett, K., Ziemniak, C., Luzuriaga, K., Capparelli, E.V., Yenokyan, G., and Persaud, D. (2015). Cell-Associated HIV-1 DNA and RNA Decay Dynamics During Early Combination Antiretroviral Therapy in HIV-1-Infected Infants. Clin. Infect. Dis. *61*, 1862–1870.

13. Vela, L.C., Carrere, L., Naasz, C., Kalavacherla, S., Tan, T.S., de Armas, L., Gao, C., Yu, X.G., Pahwa, S.G., Luzuriaga, K., and Lichterfeld, M. (2024). Profound reduction of HIV-1 reservoir cells over 3 decades of antiretroviral therapy started in early infancy. JCI Insight *10*, e186550. https://doi.org/10.1172/jci.insight.186550.

14. McMyn, N.F., Varriale, J., Fray, E.J., Zitzmann, C., MacLeod, H., Lai, J., Singhal, A., Moskovljevic, M., Garcia, M.A., Lopez, B.M., et al. (2023). The latent reservoir of inducible, infectious HIV-1 does not decrease despite decades of antiretroviral therapy. J. Clin. Investig. *133*, e171554.

15. Reeves, D.B., Duke, E.R., Wagner, T.A., Palmer, S.E., Spivak, A.M., and Schiffer, J.T. (2018). A majority of HIV persistence during antiretroviral therapy is due to infected cell proliferation. Nat. Commun. *9*, 4811.

16. Lian, X., Seiger, K.W., Parsons, E.M., Gao, C., Sun, W., Gladkov, G.T., Roseto, I.C., Einkauf, K.B., Osborn, M.R., Chevalier, J.M., et al. (2023). Progressive transformation of the HIV-1 reservoir cell profile over two decades of antiviral therapy. Cell Host Microbe *31*, 83–96.e5.

17. Lichterfeld, M., Gao, C., and Yu, X.G. (2022). An ordeal that does not heal: understanding barriers to a cure for HIV-1 infection. Trends Immunol. *43*, 608–616.

18. Sun, W., Gao, C., Hartana, C.A., Osborn, M.R., Einkauf, K.B., Lian, X., Bone, B., Bonheur, N., Chun, T.W., Rosenberg, E.S., et al. (2023). Phenotypic signatures of immune selection in HIV-1 reservoir cells. Nature *614*, 309–317.

19. Einkauf, K.B., Osborn, M.R., Gao, C., Sun, W., Sun, X., Lian, X., Parsons, E.M., Gladkov, G.T., Seiger, K.W., Blackmer, J.E., et al. (2022). Parallel analysis of transcription, integration, and sequence of single HIV-1 proviruses. Cell *185*, 266–282.e15.

20. Astorga-Gamaza, A., Perea, D., Sanchez-Gaona, N., Calvet-Mirabent, M., Gallego-Cortés, A., Grau-Expósito, J., Sanchez-Cerrillo, I., Rey, J., Castellví, J., Curran, A., et al. (2023). KLRG1 expression on natural killer cells is associated with HIV persistence, and its targeting promotes the reduction of the viral reservoir. Cell Rep. Med. *4*, 101202.

21. Armani-Tourret, M., Bone, B., Tan, T.S., Sun, W., Bellefroid, M., Struyve, T., Louella, M., Yu, X.G., and Lichterfeld, M. (2024). Immune targeting of HIV-1 reservoir cells: a path to elimination strategies and cure. Nat. Rev. Microbiol. *22*, 328–344.

22. Lee, G.Q., and Lichterfeld, M. (2022). Near-Full-Length Single-Genome HIV-1 DNA Sequencing. Methods Mol. Biol. *2407*, 357–364.

23. Einkauf, K.B., Lee, G.Q., Gao, C., Sharaf, R., Sun, X., Hua, S., Chen, S.M., Jiang, C., Lian, X., Chowdhury, F.Z., et al. (2019). Intact HIV-1 proviruses accumulate at distinct chromosomal positions during prolonged antiretroviral therapy. J. Clin. Investig. *129*, 988–998.

24. Jiang, C., Lian, X., Gao, C., Sun, X., Einkauf, K.B., Chevalier, J.M., Chen, S.M.Y., Hua, S., Rhee, B., Chang, K., et al. (2020). Distinct viral reservoirs in individuals with spontaneous control of HIV-1. Nature *585*, 261–267.

25. Yeh, Y.H.J., Yang, K., Razmi, A., and Ho, Y.C. (2021). The Clonal Expansion Dynamics of the HIV-1 Reservoir: Mechanisms of Integration Site-Dependent Proliferation and HIV-1 Persistence. Viruses *13*, 1858.

26. Liu, R., Simonetti, F.R., and Ho, Y.-C. (2020). The forces driving clonal expansion of the HIV-1 latent reservoir. Virol. J. *17*, 4.

27. Pinzone, M.R., VanBelzen, D.J., Weissman, S., Bertuccio, M.P., Cannon, L., Venanzi-Rullo, E., Migueles, S., Jones, R.B., Mota, T., Joseph, S.B., et al. (2019). Longitudinal HIV sequencing reveals reservoir expression leading to decay which is obscured by clonal expansion. Nat. Commun. *10*, 728.

28. Falcinelli, S.D., Kilpatrick, K.W., Read, J., Murtagh, R., Allard, B., Ghofrani, S., Kirchherr, J., James, K.S., Stuelke, E., Baker, C., et al. (2021). Longitudinal Dynamics of Intact HIV Proviral DNA and Outgrowth Virus Frequencies in a Cohort of Individuals Receiving Antiretroviral Therapy. J. Infect. Dis. *224*, 92–100.

29. Peluso, M.J., Bacchetti, P., Ritter, K.D., Beg, S., Lai, J., Martin, J.N., Hunt, P.W., Henrich, T.J., Siliciano, J.D., Siliciano, R.F., et al. (2020). Differential decay of intact and defective proviral DNA in HIV-1-infected individuals on suppressive antiretroviral therapy. JCI Insight *5*, e132997.

30. Carlson, J.M., Brumme, C.J., Martin, E., Listgarten, J., Brockman, M.A., Le, A.Q., Chui, C.K.S., Cotton, L.A., Knapp, D.J.H.F., Riddler, S.A., et al. (2012). Correlates of protective cellular immunity revealed by analysis of population-level immune escape pathways in HIV-1. J. Virol. *86*, 13202–13216.

31. Turk, G., Seiger, K., Lian, X., Sun, W., Parsons, E.M., Gao, C., Rassadkina, Y., Polo, M.L., Czernikier, A., Ghiglione, Y., et al. (2022). A Possible Sterilizing Cure of HIV-1 Infection Without Stem Cell Transplantation. Ann. Intern. Med. *175*, 95–100.

32. Groner, A.C., Meylan, S., Ciuffi, A., Zangger, N., Ambrosini, G., Dénervaud, N., Bucher, P., and Trono, D. (2010). KRAB-zinc finger proteins and KAP1 can mediate long-range transcriptional repression through heterochromatin spreading. PLoS Genet. *6*, e1000869.

33. Rowe, H.M., Friedli, M., Offner, S., Verp, S., Mesnard, D., Marquis, J., Aktas, T., and Trono, D. (2013). De novo DNA methylation of endogenous retroviruses is shaped by KRAB-ZFPs/KAP1 and ESET. Development *140*, 519–529.

34. Seczynska, M., Bloor, S., Cuesta, S.M., and Lehner, P.J. (2022). Genome surveillance by HUSH-mediated silencing of intronless mobile elements. Nature *601*, 440–445.

35. Collins, D.R., Urbach, J.M., Racenet, Z.J., Arshad, U., Power, K.A., Newman, R.M., Mylvaganam, G.H., Ly, N.L., Lian, X., Rull, A., et al. (2021). Functional impairment of HIV-specific CD8(+) T cells precedes aborted spontaneous control of viremia. Immunity *54*, 2372–2384.e7.

36. Gaiha, G.D., Rossin, E.J., Urbach, J., Landeros, C., Collins, D.R., Nwonu, C., Muzhingi, I., Anahtar, M.N., Waring, O.M., Piechocka-Trocha, A., et al. (2019). Structural topology defines protective CD8(+) T cell epitopes in the HIV proteome. Science *364*, 480–484.

37. Cotugno, N., Morrocchi, E., Rinaldi, S., Rocca, S., Pepponi, I., di Cesare, S., Bernardi, S., Zangari, P., Pallikkuth, S., de Armas, L., et al. (2020). Early antiretroviral therapy-treated perinatally HIV-infected seronegative children demonstrate distinct long-term persistence of HIV-specific T-cell and B-cell memory. AIDS *34*, 669–680. https://doi.org/10.1097/QAD.0000000000002485.

38. Pallmer, K., and Oxenius, A. (2016). Recognition and Regulation of T Cells by NK Cells. Front. Immunol. *7*, 251.

39. Haynes, B.F., Gilbert, P.B., McElrath, M.J., Zolla-Pazner, S., Tomaras, G.D., Alam, S.M., Evans, D.T., Montefiori, D.C., Karnasuta, C., Sutthent, R., et al. (2012). Immune-correlates analysis of an HIV-1 vaccine efficacy trial. N. Engl. J. Med. *366*, 1275–1286.

40. Wren, L.H., Chung, A.W., Isitman, G., Kelleher, A.D., Parsons, M.S., Amin, J., Cooper, D.A., ADCC study collaboration investigators, Stratov, I., Navis, M., and Kent, S.J. (2013). Specific antibody-dependent cellular cytotoxicity responses associated with slow progression of HIV infection. Immunology *138*, 116–123.

41. Lambotte, O., Ferrari, G., Moog, C., Yates, N.L., Liao, H.X., Parks, R.J., Hicks, C.B., Owzar, K., Tomaras, G.D., Montefiori, D.C., et al. (2009). Heterogenous neutralizing antibody and antibody-dependent cell cytotoxicity responses in HIV-1 elite controllers. AIDS *23*, 897–906.

42. Anderko, R.R., and Mailliard, R.B. (2023). Mapping the interplay between NK cells and HIV: therapeutic implications. J. Leukoc. Biol. *113*, 109–138.

43. Scully, E., and Alter, G. (2016). NK cells in HIV Disease. Curr. HIV AIDS Rep. *13*, 85–94.

44. López-Botet, M., Muntasell, A., and Vilches, C. (2014). The CD94/NKG2C+ NK-cell subset on the edge of innate and adaptive immunity to human cytomegalovirus infection. Semin. Immunol. *26*, 145–151.

45. Gumá, M., Angulo, A., Vilches, C., Gómez-Lozano, N., Malats, N., and López-Botet, M. (2004). Imprint of human cytomegalovirus infection on the NK cell receptor repertoire. Blood *104*, 3664–3671.

46. Nielsen, C.M., White, M.J., Goodier, M.R., and Riley, E.M. (2013). Functional Significance of CD57 Expression on Human NK Cells and Relevance to Disease. Front. Immunol. *4*, 422.

47. Sun, J.C., Beilke, J.N., and Lanier, L.L. (2009). Adaptive immune features of natural killer cells. Nature *457*, 557–561.

48. Lopez-Vergès, S., Milush, J.M., Schwartz, B.S., Pando, M.J., Jarjoura, J., York, V.A., Houchins, J.P., Miller, S., Kang, S.M., Norris, P.J., et al. (2011). Expansion of a unique CD57^{+}NKG2Chi natural killer cell subset during acute human cytomegalovirus infection. Proc. Natl. Acad. Sci. USA *108*, 14725–14732.

49. Capuano, C., Pighi, C., Battella, S., Santoni, A., Palmieri, G., and Galandrini, R. (2019). Memory NK Cell Features Exploitable in Anticancer Immunotherapy. J. Immunol. Res. *2019*, 8795673.

50. Capuano, C., Pighi, C., Battella, S., Pulcinelli, F., Santoro, C., Ferretti, A., Turriziani, O., De Federicis, D., Fionda, C., Sciumè, G., et al. (2022). (Auto) Antibody Responses Shape Memory NK Cell Pool Size and Composition. Biomedicines *10*, 625.

51. Lee, W.S., Richard, J., Lichtfuss, M., Smith, A.B., 3rd, Park, J., Courter, J.R., Melillo, B.N., Sodroski, J.G., Kaufmann, D.E., Finzi, A., et al. (2016). Antibody-Dependent Cellular Cytotoxicity against Reactivated HIV-1-Infected Cells. J. Virol. *90*, 2021–2030.

52. Lee, W.S., Kristensen, A.B., Rasmussen, T.A., Tolstrup, M., Østergaard, L., Søgaard, O.S., Wines, B.D., Hogarth, P.M., Reynaldi, A., Davenport, M.P., et al. (2017). Anti-HIV-1 ADCC Antibodies following Latency Reversal and Treatment Interruption. J. Virol. *91*, e00603-17.

53. Hartana, C.A., Garcia-Broncano, P., Rassadkina, Y., Lian, X., Jiang, C., Einkauf, K.B., Maswabi, K., Ajibola, G., Moyo, S., Mohammed, T., et al. (2022). Immune correlates of HIV-1 reservoir cell decline in early-treated infants. Cell Rep. *40*, 111126.

54. Massanella, M., Bender Ignacio, R.A., Lama, J.R., Pagliuzza, A., Dasgupta, S., Alfaro, R., Rios, J., Ganoza, C., Pinto-Santini, D., Gilada, T., et al. (2021). Long-term effects of early antiretroviral initiation on HIV reservoir markers: a longitudinal analysis of the MERLIN clinical study. Lancet Microbe *2*, e198–e209.

55. Shelton, E.M., Reeves, D.B., and Bender Ignacio, R.A. (2020). Initiation of Antiretroviral Therapy during Primary HIV Infection: Effects on the Latent HIV Reservoir, Including on Analytic Treatment Interruptions. AIDS Rev. *23*, 28–39.

56. Persaud, D., Gay, H., Ziemniak, C., Chen, Y.H., Piatak, M., Jr., Chun, T.W., Strain, M., Richman, D., and Luzuriaga, K. (2013). Absence of detectable HIV-1 viremia after treatment cessation in an infant. N. Engl. J. Med. *369*, 1828–1835.

57. Luzuriaga, K., Tabak, B., Garber, M., Chen, Y.H., Ziemniak, C., McManus, M.M., Murray, D., Strain, M.C., Richman, D.D., Chun, T.W., et al. (2014). HIV type 1 (HIV-1) proviral reservoirs decay continuously under sustained virologic control in HIV-1-infected children who received early treatment. J. Infect. Dis. *210*, 1529–1538.

58. Bengu, N., Cromhout, G., Adland, E., Govender, K., Herbert, N., Lim, N., Fillis, R., Sprenger, K., Vieira, V., Kannie, S., et al. (2024). Sustained aviremia despite anti-retroviral therapy non-adherence in male children after in utero HIV transmission. Nat. Med. *30*, 2796–2804.

59. Huang, S.-H., Ren, Y., Thomas, A.S., Chan, D., Mueller, S., Ward, A.R., Patel, S., Bollard, C.M., Cruz, C.R., Karandish, S., et al. (2018). Latent HIV reservoirs exhibit inherent resistance to elimination by CD8+ T cells. J. Clin. Investig. *128*, 876–889.

60. Bone, B., and Lichterfeld, M. (2024). "Block and lock" viral integration sites in persons with drug-free control of HIV-1 infection. Curr. Opin. HIV AIDS *19*, 110–115.

61. Dragoni, F., Kwaa, A.K., Traut, C.C., Veenhuis, R.T., Woldemeskel, B.A., Camilo-Contreras, A., Raymond, H.E., Dykema, A.G., Scully, E.P., Rosecrans, A.M., et al. (2023). Proviral location affects cognate peptide-induced virus production and immune recognition of HIV-1-infected T cell clones. J. Clin. Investig. *133*, e171097.

62. Teixeira, A.R., Bittar, C., Silva Santos, G.S., Oliveira, T.Y., Huang, A.S., Linden, N., Ferreira, I.A.T.M., Murdza, T., Muecksch, F., Jones, R.B., et al. (2024). Transcription of HIV-1 at sites of intact latent provirus integration. J. Exp. Med. *221*, e20240391.

63. Takata, H., Mitchell, J.L., Pacheco, J., Pagliuzza, A., Pinyakorn, S., Buranapraditkun, S., Sacdalan, C., Leyre, L., Nathanson, S., Kakazu, J.C., et al. (2023). An active HIV reservoir during ART is associated with maintenance of HIV-specific CD8(+) T cell magnitude and short-lived differentiation status. Cell Host Microbe *31*, 1494–1506.e4.

64. Rinaldi, S., Pallikkuth, S., Cameron, M., de Armas, L.R., Cotugno, N., Dinh, V., Pahwa, R., Richardson, B., Saini, S.R., Rocca, S., et al. (2020). Impact of Early Antiretroviral Therapy Initiation on HIV-Specific CD4 and CD8 T Cell Function in Perinatally Infected Children. J. Immunol. *204*, 540–549. https://doi.org/10.4049/jimmunol.1900856.

65. Scott, Z.A., Chadwick, E.G., Gibson, L.L., Catalina, M.D., McManus, M.M., Yogev, R., Palumbo, P., Sullivan, J.L., Britto, P., Gay, H., et al. (2001). Infrequent detection of HIV-1-specific, but not cytomegalovirus-specific, CD8(+) T cell responses in young HIV-1-infected infants. J. Immunol. *167*, 7134–7140.

66. Palma, P., Romiti, M.L., Cancrini, C., Pensieroso, S., Montesano, C., Bernardi, S., Amicosante, M., Di Cesare, S., Castelli-Gattinara, G., Wahren, B., and Rossi, P. (2008). Delayed early antiretroviral treatment is

associated with an HIV-specific long-term cellular response in HIV-1 vertically infected infants. Vaccine *26*, 5196–5201.

67. Ali, T.H., Pisanti, S., Ciaglia, E., Mortarini, R., Anichini, A., Garofalo, C., Tallerico, R., Santinami, M., Gulletta, E., Ietto, C., et al. (2014). Enrichment of CD56dimKIR+CD57+ highly cytotoxic NK cells in tumour-infiltrated lymph nodes of melanoma patients. Nat. Commun. *5*, 5639.
68. de Jonge, K., Ebering, A., Nassiri, S., Maby-El Hajjami, H., Ouertatani-Sakouhi, H., Baumgaertner, P., and Speiser, D.E. (2019). Circulating CD56bright NK cells inversely correlate with survival of melanoma patients. Sci. Rep. *9*, 4487.
69. Alter, G., Teigen, N., Davis, B.T., Addo, M.M., Suscovich, T.J., Waring, M.T., Streeck, H., Johnston, M.N., Staller, K.D., Zaman, M.T., et al. (2005). Sequential deregulation of NK cell subset distribution and function starting in acute HIV-1 infection. Blood *106*, 3366–3369.
70. Doria, M., Zicari, S., Cotugno, N., Domínguez-Rodríguez, S., Ruggiero, A., Pascucci, G.R., Tagarro, A., Rojo Conejo, P., Nastouli, E., Gärtner, K., et al. (2021). Early ART initiation during infancy preserves natural killer cells in young European adolescents living with HIV (CARMA cohort). J. Int. AIDS Soc. *24*, e25717.
71. Marras, F., Casabianca, A., Bozzano, F., Ascierto, M.L., Orlandi, C., Di Biagio, A., Pontali, E., Dentone, C., Orofino, G., Nicolini, L., et al. (2017). Control of the HIV-1 DNA Reservoir Is Associated In Vivo and In Vitro with NKp46/NKp30 (CD335 CD337) Inducibility and Interferon Gamma Production by Transcriptionally Unique NK Cells. J. Virol. *91*, e00647-17.
72. López-Botet, M., De Maria, A., Muntasell, A., Della Chiesa, M., and Vilches, C. (2023). Adaptive NK cell response to human cytomegalovirus: Facts and open issues. Semin. Immunol. *65*, 101706.
73. Hearps, A.C., Zhou, J., Agius, P.A., Ha, P., Lee, S., Price, P., Kek, H., Kroon, E., Akapirat, S., Pinyakorn, S., et al. (2024). Adaptive NK Cells Rapidly Expand during Acute HIV Infection and Persist Despite Early Initiation of Antiretroviral Therapy. J. Immunol. *212*, 1553–1563.
74. Dufour, C., Ruiz, M.J., Pagliuzza, A., Richard, C., Shahid, A., Fromentin, R., Ponte, R., Cattin, A., Wiche Salinas, T.R., Salahuddin, S., et al. (2023). Near full-length HIV sequencing in multiple tissues collected postmortem reveals shared clonal expansions across distinct reservoirs during ART. Cell Rep. *42*, 113053.
75. Daniel Scott-Algara CD, V. Arnold, J.-S. Cummings, F. Boufassa, O. Lambotte, L. Hocqueloux, A. Sáez-Cirión, C. Rouzioux, editor Post-Treatment Controllers Have Particular NK Cells With High Anti-HIV Capacity: VISCONTI Study. Conference on Retroviruses and Opportunistic Pathogens; 2015; Seattle, WA.
76. Etemad, B., Sun, X., Li, Y., Melberg, M., Moisi, D., Gottlieb, R., Ahmed, H., Aga, E., Bosch, R.J., Acosta, E.P., et al. (2023). HIV post-treatment controllers have distinct immunological and virological features. Proc. Natl. Acad. Sci. USA *120*, e2218960120.
77. Garcia-Broncano, P., Maddali, S., Einkauf, K.B., Jiang, C., Gao, C., Chevalier, J., Chowdhury, F.Z., Maswabi, K., Ajibola, G., Moyo, S., et al. (2019). Early antiretroviral therapy in neonates with HIV-1 infection restricts viral reservoir size and induces a distinct innate immune profile. Sci. Transl. Med. *11*, eaax7350.
78. Folks, T.M., Powell, D., Lightfoote, M., Koenig, S., Fauci, A.S., Benn, S., Rabson, A., Daugherty, D., Gendelman, H.E., and Hoggan, M.D. (1986). Biological and biochemical characterization of a cloned Leu-3- cell surviving infection with the acquired immune deficiency syndrome retrovirus. J. Exp. Med. *164*, 280–290.
79. Baba, M., Miyake, H., Okamoto, M., Iizawa, Y., and Okonogi, K. (2000). Establishment of a CCR5-expressing T-lymphoblastoid cell line highly susceptible to R5 HIV type 1. AIDS Res. Hum. Retroviruses *16*, 935–941.
80. Folks, T., Benn, S., Rabson, A., Theodore, T., Hoggan, M.D., Martin, M., Lightfoote, M., and Sell, K. (1985). Characterization of a continuous T-cell line susceptible to the cytopathic effects of the acquired immunodeficiency syndrome (AIDS)-associated retrovirus. Proc. Natl. Acad. Sci. USA *82*, 4539–4543.
81. Platt, E.J., Wehrly, K., Kuhmann, S.E., Chesebro, B., and Kabat, D. (1998). Effects of CCR5 and CD4 cell surface concentrations on infections by macrophagetropic isolates of human immunodeficiency virus type 1. J. Virol. *72*, 2855–2864.
82. Bruner, K.M., Wang, Z., Simonetti, F.R., Bender, A.M., Kwon, K.J., Sengupta, S., Fray, E.J., Beg, S.A., Antar, A.A.R., Jenike, K.M., et al. (2019). A quantitative approach for measuring the reservoir of latent HIV-1 proviruses. Nature *566*, 120–125.
83. Wagner, T.A., McLaughlin, S., Garg, K., Cheung, C.Y.K., Larsen, B.B., Styrchak, S., Huang, H.C., Edlefsen, P.T., Mullins, J.I., and Frenkel, L.M. (2014). Proliferation of cells with HIV integrated into cancer genes contributes to persistent infection. Science *345*, 570–573.
84. Rocca, S., Zangari, P., Cotugno, N., De Rossi, A., Ferns, B., Petricone, D., Rinaldi, S., Giaquinto, C., Bernardi, S., Rojo, P., et al. (2019). Human Immunodeficiency Virus (HIV)-Antibody Repertoire Estimates Reservoir Size and Time of Antiretroviral Therapy Initiation in Virally Suppressed Perinatally HIV-Infected Children. J. Pediatric Infect. Dis. Soc. *8*, 433–438.

STAR★METHODS

KEY RESOURCES TABLE

REAGENT or RESOURCE	SOURCE	IDENTIFIER
Antibodies		
Anti-CD28 Clone CD28.2	BD Pharmigen	Cat # 555725; RRID:AB_396068
Anti-CD49d Clone 9F10	Invitrogen	Cat # 14-0499-82; RRID:AB_467292
Anti-CD40 Clone EA-5	Merck	Cat # 217590; RRID:AB_2260140
CD10 BV510 Clone HI10a	BD	Cat # 563032 RRID:AB_2737964
BD Horizon Fixable Viability Stain 510	BD	Cat # 564406
CD3 BV510 Clone UCHT1	BD	Cat # 563109 RRID:AB_2738909
CD21 APC Clone B-ly4	BD	Cat # 559867 RRID:AB_10679119
CD27 FITC Clone M-T271	BD	Cat # 555440 RRID:AB_395833
CD38 PE-Cy7 Clone HB7	BD	Cat # 335825 RRID:AB_1727473
IgD BV421 Clone IA6-2	BD	Cat # 565940 RRID:AB_11153121
IgM PE-CF594 Clone G20-127	BD	Cat # 562539 RRID:AB_11152645
IgG BV605 Clone G18-145	BD	Cat # 563032 RRID:AB_2738092
CXCR5 BV605 Clone RF8B2	BD	Cat # 740379 RRID:AB_394339
CD4 APC-Cy7 Clone RPA-T4	BD	Cat # 557871 RRID:AB_396913
CD19 APC-R700 Clone SJ25C1	BD	Cat # 659121 RRID:AB_1645728
CD45RO PE-Cy5 Clone UCHL1	Biolegend	Cat # 304208 RRID:AB_2564160
CD56 PerCP-Cy5.5 Clone NCAM-1	BD	Cat # 560842 RRID:AB_2033964
CD16 BV510 Clone 3G8	BD	Cat # 563830 RRID:AB_2744296
CD3 PE-CF594 Clone UCHT1	BD	Cat # 562280 RRID:AB_11153674
CD14 BV605 Clone M5E2	BD	Cat # 564054 RRID:AB_2687593
CD57 APC Clone NK-1	BD	Cat # 560845 RRID:AB_10563760
DNAM-1 BV786 Clone DX11	BD	Cat # 742497 RRID:AB_2740830
CD19 APC Alexa Fluor 750 Clone SJ25-C1	Life Technologies	Cat # MHCD1927 RRID:AB_10373380
NKG2C PE Clone REA205	Myltenyi Biotec	Cat # 130-119-776
NKp46 PE-Cy7 Clone 9E2	BioLegend	Cat # 331916
Granzyme B BV421 Clone GB11	BD	Cat # 563389 RRID:AB_2738175
Perforin BV421 Clone δG9	BD	Cat # 563393 RRID:AB_396418
CD107a FITC Clone H4A3	BD	Cat # 555800 RRID:AB_396134
IFN- γ BV650 Clone 4S.B3	BD	Cat # 563416 RRID:AB_2738193
TNF- α Alexa Fluor 700 Clone Mab11	BioLegend	Cat # 502928 RRID:AB_396978
p24 PE Clone KC57-RD1	Beckman Coulter	Cat # 6604667
Biological samples		
PBMCs from study participants living with HIV	LeukoHIV cohort - Bambino Gesù Children's Hospital	https://www.ospedalebambinogesu.it/about-us-169889/
Plasma from study participants living with HIV	LeukoHIV cohort - Bambino Gesù Children's Hospital	https://www.ospedalebambinogesu.it/about-us-169889/
Chemicals, peptides, and recombinant proteins		
Ficoll-Paque PLUS	Cytiva	Cat # 17144003
FBS	Gibco	Cat #10270-106
DMSO	Sigma	Cat #D8418
RPMI 1640	Euroclone	Cat # ECM9106L
1% Pen/Strep	Euroclone	Cat # ECB3001D
L-Glutammine 100x	Euroclone	Cat # ECB3000D
KLH (Hemocyanin from Megathura crenulate)	Sigma	Cat #H8283-50MG

(*Continued on next page*)

Continued

REAGENT or RESOURCE	SOURCE	IDENTIFIER
SEB (Staphylococcus Enterotoxin B)	Sigma	Cat #S4881-5MG
Gag-pte pools	NIH-ARP	Cat # ARP-12437
Env-pte pools	NIH-ARP	Cat # ARP- 12698
Gp140	NISBC	Cat # UG37_020714A
2% formaldehyde	Sigma	Cat # HT5014-120ML
Triton	Biorad	X100-500ML
Golgi Stop (Protein Transport Inhibitor containing monensin)	BD	51-2092KZ
BD PERM II	BD	340973
BFA (Brefelfin A)	Sigma	B7450
EDTA	Sigma	324506-100ML
Cell Proliferation Dye (CPD) eFluor450	e-Bioscience	65–0842
LIVE/DEAD Fixable Near-IR Dead Cell stain dye	Invitrogen	Cat #L34976A
Cell Proliferation Dye (CPD) eFluor670	e-Bioscience	65–0840
ddPCR Supermix for probes (no dUTP)	Bio-Rad	Cat # 186-3024
Platinum *Taq* polymerase	ThermoFisher Scientific	Cat # 10966018
Platinum SuperFi II PCR master mix	ThermoFisher Scientific	Cat # 12368050
AMPure XP bead reagent	Beckman Coulter	Cat # A63881
DMEM/F-12	ThermoFisher Scientific	Cat# 10565042
Phytohaemagglutinin	ThermoFisher Scientific	R30852801
Recombinant IL-2	NIH-ARP	ARP0901
Buffer RLT Plus	Qiagen	Cat#1053393
Invitrogen Dynabeads	ThermoFisher Scientific	Cat#65002
Invitrogen SUPERase-In RNase Inhibitor	ThermoFisher Scientific	Cat#AM2694
Invitrogen dNTP mix (10mM each)	ThermoFisher Scientific	Cat#18427088
Superscript™ II Reverse Transcriptase	ThermoFisher Scientific	Cat#18064014
Critical commercial assays		
FLUROSPOT T	AID	Cat # ELSP5810
Western Blot kit 2.2	MP Biomedicals Germany GmbH	Cat # 11030-036
DNeasy Blood and Tissue kit	Qiagen	Cat # 69504
Britelite plus Reporter Gene Assay System	revvity	6066766
Lightning-Link® R-PE Conjugation Kit	Abcam	Cat # ab102918
KAPA HiFi HotStart ReadyMix	Roche	Cat#7958935001
REPLI-g Single Cell Kit	Qiagen	Cat#150345
Stemcell EasySep Human $CD4^+$ T cell Isolation Kit	Stemcell Technologies	Cat#17952
Experimental models: Cell lines		
8E5/LAV (HIV1) cell line	NIH-ARP	ARP0110
ACH-2 cell line	NIH-ARP	ARP0138
TZM-bl cell line	NIH-ARP	ARP5011
MOLT-4/CCR5 cell line	NIH-ARP	ARP5039
Oligonucleotides		
See Table S5 for primer and probe sequences	IDT	N/A
Software and algorithms		
BioRender	BioRender	N/A
Genious Prime 2023.2.1	Biomatters	N/A
Prism 10	GraphPad	N/A
R	R Core Team	N/A
Automated in-house proviral intactness	Lee et al. [22]	N/A
FlowJo (version 10.10.0.)	Tree Star LLC	N/A

(*Continued on next page*)

Continued

REAGENT or RESOURCE	SOURCE	IDENTIFIER
QuantaSoft software	Bio-Rad	N/A
ImageJ software (1.52v)	NIH	N/A
MEGA11	MEGA	N/A
CytExpert 2.0	Beckman Coulter Life Sciences	
BD FACSDiva Software v8.0.1	BD Biosciences	
AID EliSpot v7 software	AutoImmun Diagnostika GmbH	
Other		
Countess II Automated Cell Counters	ThermoFisher Scientific	N/A
BD FACSAria III Flow Cytometer	BD	N/A
CytoFLEX Flow Cytometer	CytoFLEX Flow Cytometer Beckman Coulter Life Sciences	N/A
ELISPOT Reader	AID	N/A
T100 Thermal cycler	Bio-Rad	N/A
QX200 ddPCR system	Bio-Rad	N/A
Tecan Microplate reader	Tecan	N/A
Illumina MiSeq performed by MGH CCIB DNA Core facility	Illumina/MGH CCIB DNA Core	N/A

EXPERIMENTAL MODEL AND STUDY PARTICIPANT DETAILS

LeukoHIV cohort

This is a non-pharmacological, cross-sectional study enrolling subjects at Bambino Gesù Children's Hospital, IRCSS, Rome, Italy. Clinical characteristics of the participants are provided in Table 1. All patients were on suppressive ART at enrollment and 4 out of nine participants presented no history of viral rebound for the previous 14 years. Occurrence of CMV infection at birth was known and experimentally confirmed in 2 out of nine participants, however CMV seropositivity was reported in 5 out of nine patients in the cohort. Gender was self-reported and the influence of gender was not measured in this study due to low sample size. PBMCs were collected according to protocols approved by the Bambino Gesù Children Hospital IRCCS, Ethical committee (protocol: 2555_OPBG_2021). Informed written consent was obtained from all study participants or from their parents/legal representatives, prior to participation.

Cell lines

Four cell lines were used in our experiments: 8E5/LAV, MOLT4/CCR5, ACH2 and TZM-bl. All cell lines were obtained from the Center for AIDS Reagents (CFAR) and listed in the key resources table. The 8E5/LAV cell line is a human lymphoblastic leukemia clone containing a single defective HIV provirus. The single integrated copy of proviral DNA directs the synthesis of all major viral structural proteins, except p64. The immunoblot of the 8E5 clone, using pooled AIDS sera, revealed the presence of virus-encoded gp120, p55, p41 and p25 and the absence of the prominent 64kD and fainter 34kD proteins. The presence of a reactive 50kD band, representing a truncated form of the 64kD polypeptide was also identified in productively infected cells. [78] The MOLT4/CCR5 cell line is a T lymphoblastoid cell line engineered to express CCR5, making it highly permissive to HIV-1 infection. [79]The ACH2 cell line is a T cell clone infected with the LAI strain of HIV-1. Each cell contains a single integrated copy of HIV-1. [80] The TZM-bl cell line is a HeLa-derived reporter cell line that highly expresses CCR5 and CD4, making it very permissive to infection. Integrated copies of luciferase and β-galactosidase genes were introduced for the detection of HIV infection through expression of those gene products. [81] 8E5/LAV cells were thawed in 10 mL of complete RPMI 1640 medium (cRPMI, supplemented with 10% FBS, 1% L-glutamine and 1% Pen/Strep) and incubated at 37°C with 5% CO2 for a maximum of two consecutive months. To ensure optimal conditions, the cRPMI was refreshed every 2-3 days to provide fresh nutrients. ACH2 and MOLT-4/CCR5 cells were maintained in R10 medium (RPMI 1640 supplemented with 10% FBS, 1% pen/strep and 1% L-glut). The TZM-bl cell line was maintained in DMEM/F-12 supplemented with 10% FBS, 1% pen/strep and 1% L-glut. Cell morphology, viability and potential contamination were regularly monitored using an optical microscope, and cells were routinely tested for mycoplasma contamination using the EZ-PCR Mycoplasma test kit.

METHOD DETAILS

Leukapheresis

We performed mononuclear cell collection of 9 HIV study participants (7 females and 2 males) with a median weight of 53.5 kg (range 42–80 kg). 12 CMNCs were performed using Optia Spectra - Terumo cell separator, in 130 min (range 101–200) with a flow rate of 35 mL/min (range 30–50 mL/min). All collections required a total blood volume of 4181 mL (range 2658–9644 mL) to be processed

using the Acid-Citrate-Dextrose Anticoagulant (ACD-A) with a median volume of 518 mL (range 394–1070 mL). All procedures were well tolerated and no side effects were recorded. Routine blood test were performed before and after the procedure and results are presented in Table S1 and no major changes in hemoglobin or total white blood cells or other parameters were observed in the group.

Sample collection outputs are presented in Table S2. PBMCs were separated by Ficoll-Paque PLUS (Cat #17144003, Cytiva Sweden AB, SE-751 84 Uppsala, Sweden) density gradient centrifugation. Countess II Automated Cell Counters (ThermoFisher Scientific, Waltham, MA, USA) was used to determine the total number of live cells, then PBMCs were cryopreserved in fetal bovine serum (FBS, Cat #10270-106, Gibco, Life technologies, Carlsbad, CA, USA) + 10% dimethyl sulfoxide (DMSO, Cat #D8418, Sigma) in liquid nitrogen until analysis.

DNA extraction

Genomic DNA (gDNA) extraction was performed on thawed PBMCs using the Qiagen DNeasy blood and tissue commercial kit.

Reservoir quantification estimation

For non-subtype B proviruses, we estimated the frequency of HIV-1 proviral copies through droplet digital PCR (ddPCR) of the 5′-LTR region. For estimating the frequency of subtype B proviruses we performed the intact proviral DNA assay (IPDA) - a multiplexed ddPCR assay that targets the Gag and Env regions, allowing for discrimination between intact or defective proviruses. Primer sequences used as well as the analysis workflow performed on the IPDA data have been previously described. [82] ddPCR targeting the *rpp30* gene allowed for a sample's cell frequency, used in downstream assays, to be determined.

HIV-1 near full-length amplification and sequencing

Near full-length amplification of HIV-1 was achieved by performing the full-length individual provirus sequencing (FLIP-seq) or matched integration site and proviral sequencing (MIP-seq) assays that we have previously described. [22,23] Briefly, ddPCR estimates of the reservoir inform a dilution of HIV-1 that is conducted to achieve a single HIV-1 genome resolution based on Poisson distribution statistics. For MIP-seq, a phi29 polymerase dependent whole genome amplification was then performed. Near full-length amplification of the HIV-1 genome (HXB2 coordinates: 638–9632) is then facilitated through PCR using nested primers (sequences previously published in [22]) and either the Platinum Taq or Platinum SuperFi Taq polymerases (Invitrogen). The size of the PCR products was clarified by DNA gel electrophoresis, with suitable products purified using AMPure XP bead-based reagent (Beckman Coulter) and sequenced using the Illumina MiSeq platform at the MGH DNA core facility. Short reads were *de novo* assembled, aligned to HXB2 and evaluated for viral fitness using a custom bioinformatics pipeline. HIV-1 proviruses that lacked lethal mutations were considered 'genome-intact', with multiple sequence alignments performed using the MUSCLE algorithm and maximum-likelihood phylogenetic trees were created using the MEGA11 software. Sequences were considered clonal if they were completely identical. Sequences that differed by a single base pair were annotated accordingly. Presented frequencies of intact or defective sequences were informed through these assays, with values below the limit of detection annotated on the data graphs. A complete overview of the FLIP and MIP sequencing performed on the LeukoHIV cohort is presented in Table S3, as well as the QVOA analysis. Clinical characteristics of the m-ART and EC comparison cohorts are summarised and presented in Table S4.

Integration site analysis

Integration site loop amplification (ISLA) is a five stage PCR workflow that we used to acquire integration sites of the HIV-1 proviruses from samples we initially performed whole genome amplifications on, as part of the MIP-seq assay. [23,83] ISLA products were purified using AMPure XP bead-based reagent (Beckman Coulter) and subjected to Illumina Miseq sequencing. Paired end FastQ files were demultiplexed, small reads were aligned to the HXB2 and GRCh38 reference genomes for HIV-1 and human respectively. Integration site coordinates were identified bio-computationally using methods previously described, [23] with these coordinates mapped to the genome using the UCSC Genome Browser to obtain host gene designations that were paired to the viral sequence.

Analysis of transcriptional behavior of HIV-1 proviruses

For analysis of specific proviral transcriptional activity, we performed parallel RNA, integration sites and proviral sequencing (PRIP-seq) as previously described. [19] PBMCs are diluted down to a single infected cell resolution and lysed with buffer RLT plus before gDNA and RNA were separated. This was facilitated through the use of magnetic streptavidin beads linked to biotinylated primers targeting the Poly-A, tat-rev, nef, pol and long LTR regions of HIV-1 RNA. RNA was separated from gDNA according to the previously described G&T protocol and then subjected to reverse transcription using Superscript II reverse transcriptase (Invitrogen) according to the manufacturer's instructions. cDNA was amplified by PCR using a modified Smart-seq2 protocol, with KAPA HiFi HotStart ReadyMix (Roche) and ISPCR primer. Quantification of transcripts was performed by ddPCR targeting the transcript regions specified by the magnetic beads. Isolated gDNA was bound to AMPure XP bead reagent for washing, then subjected to a whole genome amplification before the MIP-seq protocol was carried out to facilitate parallel proviral sequencing and integration site analysis that can be paired to the proviral transcriptional behavior.

In vitro quantification of the replication competent reservoir

$CD4^+$ T cells were first isolated from whole PBMCs and diluted down to a single replication-competent virus infected cell level, according to FLIP-seq data. Cells were stimulated with phytohemagglutinin (PHA) (1 $\mu g ml^{-1}$) and incubated with IL-2 and irradiated feeder PBMCs in R1xx0/1xx00 media (IL-2 concentration in media was 100 U/mL). ACH-2 cells (NIH) and MOLT-4/CCR5 cells (NIH) were used as positive and negative controls respectively and maintained beforehand in R10 medium. These cell lines received the same stimulation in PHA-containing R10/100. On day 4, PHA-containing medium was removed, cells were washed in PBS and uninfected MOLT-4/CCR5 cells were added to the culture wells, with media changes every other day until the time points of day 14 and day 21 were reached. On the respective time points, culture supernatants were aliquoted onto cultured TZM-bl cells (NIH) and allowed to incubate for 2 days. Presence of replication competent in the supernatant was then detected by tat-dependent BriteLite luciferase assay (Britelite plus) using a Tecan Plate reader. Outgrowth of replication competent viruses was defined as a reading 5-fold higher than the negative control. Cells from wells with positive outgrowth were then transferred to the bottom of transwells (Corning), with uninfected MOLT-4/CCR5 cells plated onto transwell inserts. After 4 days of culture, MOLT-4/CCR5 cells were harvested and subjected to FLIP-seq.

IFN-γ/IL-2 FluoroSpot T cell assays

IFN-ɣ/IL-2 FluoroSpot (AID, Straβberg, Germany) assays were performed according to the manufacturer's instructions. Briefly, 0.3 to 3.0 × 105 thawed PBMCs, post 2 h recovery at 37°C, were incubated in 96-well plates pre-coated with monoclonal capture antibodies against IFN-ɣ and IL-2 (AID, Straβberg, Germany) seeded with anti-CD28 (1 μg/mL, BD Pharmigen, Clone CD28.2), anti-CD49d (1 μg/ml, Invitrogen, Clone 9F10), anti-CD40 (1 μg/mL, Merck, Clone EA-5) antibodies and contained RPMI medium (RPMI 1640, Cat #ECM9106L, Euroclone) + 10% FBS (FBS, Cat #10270-106, Gibco) + 1% Pen/Strep (Cat # ECB3001D Euroclone) and L-Glu (Cat # ECB3000D Euroclone) supplemented with 0.5 μg of Hemocyanin from Megathura crenulata (KLH, Sigma) as a negative control, 200 ng/mL Staphylococcus Enterotoxin B (SEB, Sigma) as a positive control, 2 μg/mL of Gag-pte or Env-pte pools (obtained from NIH-ARP) as specific antigens. Plates were incubated for 18–20 h at 37°C 5% carbon dioxide (CO_2) and then washed with washing buffer. After incubation, the detection antibodies (anti-IL-2 biotin and anti-IFN-ɣ-FITC) were added to each well and incubated for 2 h at room temperature (RT). Then streptavidin red-conjugate and anti-FITC green were added and another 1 h of incubation was needed. Finally, fluorescence enhancer was loaded and read by a ELISPOT reader (AID iSpot, Straβberg, Germany). T cells secreting single IFN-ɣ (FITC/green spots) single IL-2 (Cy3/red spots) and dual IFN-ɣ/IL-2 (merged/yellow spots) were counted using AID EliSpot v7 software (Autoimmun Diagnostika GmbH, Straβberg, Germany) normalized for the number of plated PBMCs and expressed as spot-forming cells/million of PBMCs. The background spot-forming cells in negative and positive control wells should be $\leq$ 10 spots and $\geq$20 spots, respectively. Otherwise, it would be considered as an indeterminate result. Laboratory personnel who conducted the assays and researchers who interpreted the results were all blind to clinical data.

HIV-1 epitope-specific $CD8^+$ T cell response mapping by IFN-γ elispot

Frozen PBMCs were thawed at 37°C and recovered in RPMI media (Sigma-Aldrich) supplemented with 10% fetal bovine serum (FBS, Sigma; R10) overnight, then resuspended at 1 × 10^6/mL in R10 and plated 200 μL per well in Immobilon-P 96-well microtiter plates (Millipore) pre-coated with 2 μg/mL anti-IFN-γ (clone DK1, Mabtech). Individual HLA-optimal HIV peptides matched to each subject's *HLA* genotype, as listed previously, [26] were added at 1 μM and incubated at 37°C overnight. Alternatively, overlapping peptide pools for Gag, Pol, Env, Nef (NIH AIDS Reagent Program) or CMV/EBV/Flu (CEF Extended Peptide Pool, Mabtech) were added at 1 μM. Triplicate negative control wells did not receive peptide and positive control wells were treated with 1 μg/mL anti-CD3 (clone OKT3, Biolegend) and 1 μg/mL anti-CD28 (clone CD28.8, Biolegend) antibodies. ELISPOT assay was performed using manufacturer's protocol with anti-IFN-γ (clone 1-DK1, Mabtech) capture, biotinylated anti-IFN-γ (clone B6-1, Mabtech) detection, Streptavidin-ALP (Mabtech) and AP Conjugated Substrate (BioRad) followed by disinfection with 0.05% Tween 20 (Thermo Fisher) and analysis using S6 Macro Analyzer (CTL Analyzers). Responses greater than 10 spots per well (50 spots per 10^6 PBMCs) and 3-fold above negative controls were scored as positive.

HIV-1 epitope-specific CD8 T cell proliferation assay

Frozen PBMCs were thawed at 37°C and recovered in RPMI media (Sigma-Aldrich) supplemented with 10% fetal bovine serum (FBS, Sigma; R10) overnight, then stained at 37°C for 20 min with 0.5 μM CellTrace CFSE (Thermo Fisher) as per manufacturer's protocol. Cells were quenched and washed twice with R10 media, then resuspended at 1 × 10^6/mL in R10 and plated at 200 μL per well in 96-well round-bottom polystyrene plates (Corning). Individual HLA-optimal HIV peptides matched to each subject's *HLA* genotype, as listed previously, [26] were added at 1 μM and incubated at 37°C for 6 days before flow cytometric assessment. Triplicate negative control wells did not receive peptide and positive control wells received 1 μg/mL anti-CD3 (clone OKT3, Biolegend) and 1 μg/mL anti-CD28 (clone CD28.8, Biolegend) antibodies. On day 6, cells were stained using Live/Dead Violet viability dye (Thermo Fisher), AlexaFluor700-*anti*-CD3 (clone SK7, Biolegend), and APC-*anti*-CD8 (clone RPA-T8, Biolegend), then analyzed by flow cytometry. Responses greater than 1% CFSE-low and 3-fold above negative controls were scored as positive.

HIV Ab western blot

Plasma samples were tested as previously described [12]. HIV Western Blot (WB) kit 2.2 (MP Biomedicals Germany GmbH) was used, following the manufacturer's instructions, to detect in 20 μL of plasma, antibodies (Abs) against 9 different HIV-1 viral proteins (gp160, gp120, p66, p55/p51, gp41, p39, p31, p24, and p17) as previously described [13]. All of the WB strips were analyzed using the ImageJ software (ImageJ 1.52v; National Institutes of Health). A score of 1 was assigned when the intensity of the band was ≥50% of that found in the strong positive control for the same antigen, whereas 0.5 was assigned when the band intensity ranged from 10% to 49% of that found in the positive control. Finally, negative results (score = 0) were assigned for band intensity ranging from 0% to 9% of that found in the positive control. A WB score was assigned to each participant by adding up the number of positive [1] and weak (0.5) responses (from 0 to 9). [43,84] HIV Ab western blot referring to samples collected in 2022 are reported in Figure S7.

Ag specific T and B cell detection by flow cytometry

In order to detect Ag specific T cells, PBMCs were resuspended at 10×10^6 cells/mL and 2.0×10^6 cells were incubated for 16 h at 37°C 5% CO_2 in 96-well U-bottom cell culture plates with anti-CD40L (PE conjugate, clone TRAP-1, BD) in R10 medium supplemented with anti-CD28 (1 μg/mL, Clone CD28.2, BD) plus DMSO, Gag- or Env-peptide pools (2 μg/mL, obtained from NIH-ARP) or staphylococcal enterotoxins B (SEB, 4 μg/mL, Sigma). Following specific stimulation, PBMCs were stained for 15 min at RT with the BD Horizon Fixable Viability Stain 510 (BD) and 20 min at 4°C for the surface expression of CD3 (BV510 conjugate, clone UCHT1) CD10 (BV510 conjugate, clone HI10a) CD16 (BV510 conjugate, clone 3G8) CD19 (APC-R700 conjugate, clone SJ25C1) CD21 (APC conjugate, clone B-ly4) CD27 (FITC conjugate, clone M-T271) CD38 (PE-Cy7 conjugate, clone HB7) IgD (BV421 conjugate, clone IA6-2) IgM (PE-CF594, clone G20-127) and IgG (BV605 conjugate, clone G18-145) (all from BD Biosciences, San Jose, CA, USA). In addition, PE-conjugated HIV-1 envelope trimeric gp140 protein was included in the panel. The gp140 protein was obtained from the NIH AIDs Reagents Program and Lightning-Link R-PE Conjugation Kit (Innova Biosciences) was used to obtain a labeled gp140-PE. For T cell phenotype the following monoclonal antibodies were used: anti-CD3 (PE-CF594 conjugate, clone UCHT1) CD27 (FITC conjugate, clone M-T271) CD10 (BV510 conjugate, clone HI10a) CXCR5 (BV605 conjugate, clone RF8B2) IgD (BV421 conjugate, clone IA6-2) CD4 (APC-Cy7 conjugate, clone RPA-T4) CD21 (APC conjugate, clone B-ly4) CD19 (APC-R700 conjugate, clone SJ25C1) (all from BD Biosciences, San Jose, CA, USA) and CD45R0 (PE-Cy5 conjugate, clone UCHL1, Biolegend). Gating strategy in Figure S2. Samples were acquired on a BD FACSAria III Flow Cytometer (BD) and data were analyzed using the FlowJo software version 10.10.0.

NK cell immunophenotyping

Cryopreserved PBMCs were thawed and stained, post 2 h recovery at 37°C, with the LIVE/DEAD Fixable Near-IR Dead Cell stain dye (from Invitrogen, Waltham, MA) for 15 min at RT. Cells were then fixed for 20 min at RT with 2% formaldehyde (Sigma), and then stained for 20 min at 4°C with the following antibodies: CD56 (PerCP-Cy5.5 conjugate, clone NCAM-1) CD16 (BV510 conjugate, clone 3G8) CD3 (PE-CF594 conjugate, clone UCHT1) CD14 (BV605 conjugate, clone M5E2) CD57 (APC conjugate, clone NK-1) DNAM-1 (BV786 conjugate, clone DX11) (all from BD Biosciences, San Jose, CA, USA) CD19 (APC Alexa Fluor 750 conjugate, clone SJ25-C1; Life Technologies, Carlsbad, CA, USA) NKG2C (PE conjugate, clone REA205; Miltenyi Biotec, Bergisch Gladbach, DE) and NKp46 (PE-Cy7 conjugate, clone 9E2, BioLegend, San Diego, CA, USA). Stained cells were permeabilized with a solution of PBS +2% FBS +0.05% Triton (Biorad) for 20 min at RT and stained for 30 min at 4°C with BV421-conjugated anti-Granzyme B (clone GB11) and -Perforin (clone δG9) mAbs (both from BD Biosciences, San Jose, CA, USA). Gating strategy is showed in Figure S4. Samples were acquired at a CytoFLEX Flow Cytometer (Beckman Coulter Life Sciences) and data were analyzed using the FlowJo software version 10.10.0.

Antibody-dependent cellular cytotoxicity (ADCC)

Antibody dependent NK cell activation assays were performed, as previously described [84] by measuring intracellular IFN-ɣ and surface CD107a expression on PBMCs used as effectors (E) against HIV-1 infected 8E5/LAV target (T) cells (obtained from NIH-ARP) in the presence of heat inactivated autologous (pHIVauto) or heterologous (pHIVhetero) HIV-1 infected plasma. Briefly, thawed effector cells, post 18 h recovery at 37°C, were incubated with an anti-CD107a antibody (FITC conjugate, clone H4A3; BD Pharmingen, San Diego, CA, USA) and target cells, at E:T ratio of 1:1 in a 96-well U-bottom cell culture plate, in the presence of heat inactivated (at 56°C for 1h) HIV-1 infected (HIVpos, dilution 1:100) or uninfected (HIVneg, dilution 1:100) plasma or no plasma. The plate was centrifuged at 300 x g for 1 min before a 6 h incubation at 37°C 5% CO_2. After the first hour, 0.66 μL/mL of BD GolgiStop (Protein Transport Inhibitor containing monensin; BD) and 10 μg/mL of brefeldin A (BFA; Sigma) were added. After stimulation, cells were washed with PBS +1% FCS +5 mM EDTA (Sigma) to promote conjugate disruption and stained with the LIVE/DEAD Fixable Near-IR Dead Cell stain dye (from Invitrogen, Waltham, MA) for 15 min at RT. Before fixing for 20 min at RT with 2% formaldehyde (Sigma) cells were stained 20 min at 4°C for the surface expression of CD56 (PerCP-Cy5.5 conjugate, clone) CD16 (BV510 conjugate, clone 3G8) CD3 (PE-CF594 conjugate, clone UCHT1) CD14 (BV605 conjugate, clone M5E2) CD57 (APC conjugate, clone NK-1) DNAM-1 (BV786 conjugate, clone DX11) (all from BD Biosciences, San Jose, CA, USA) CD19 (APC Alexa Fluor 750 conjugate, clone SJ25-C1; Life Technologies, Carlsbad, CA, USA) NKG2C (PE conjugate, clone REA205; Miltenyi Biotec, Bergisch Gladbach, DE) and NKp46 (PE-Cy7 conjugate, clone 9E2; BioLegend, San Diego, CA, USA). Stained cells were permeabilized with a solution of PBS +2% FBS +0.05% Triton (Biorad) for 20 min at RT and stained for 30 min at 4°C for the intracellular expression of IFN-ɣ (BV650 conjugate, clone 4S.B3)

granzyme B (BV421 conjugate, clone GB11) and perforin (BV421 conjugate, clone δG9) (all from BD Biosciences, San Jose, CA, USA) and TNF-α (Alexa Fluor 700 conjugate, clone Mab11; BioLegend, San Diego, CA, USA). Gating strategy is showed in Figure S4. Samples were acquired on a CytoFLEX Flow Cytometer (Beckman Coulter Life Sciences) and data were analyzed using the FlowJo software version 10.10.0.

Infected cell elimination assays

PBMCs were used as effectors (E) against HIV-1 infected 8E5/LAV target (T) cells in the presence of heat-inactivated autologous (pHIVauto) or heterologous (pHIVhetero) HIV-1 infected plasma, being the percentage (%) of killing calculated through the intracellular p24 expression. Briefly, thawed Cell Proliferation Dye (CPD) eFluor450 (eBioscience)-labeled effector cells were incubated with CPD eFluor670 (eBioscience)-labeled target cells, at E:T ratio 1:1 in a 96-well U-bottom cell culture plate, in the presence of HIV-1 infected (HIVpos) or uninfected (HIVneg) plasma or no plasma. The plasma samples were first heat inactivated at 56°C for 1 h and added at dilution 1:100. The plate was centrifuged at 300 x g for 1 min before a 6 h incubation at 37°C 5% CO_2. After stimulation, cells were washed with PBS +1% FCS + 5mM EDTA to promote conjugate disruption, stained for 15 min at RT with the LIVE/DEAD Fixable Near-IR Dead Cell stain dye (Invitrogen, Waltham, MA) fixed for 20 min at RT with 1% formaldehyde (Sigma) and permeabilized for 20 min at RT with 1X BD FACS Permeabilizing Solution II (BD). After permeabilization, cells were stained 30 min at 4°C for the intracellular expression of p24 (PE conjugate, clone KC57-RD1; Beckman Coulter). Samples were acquired on a CytoFLEX Flow Cytometer (Beckman Coulter Life Sciences) and data were analyzed using the FlowJo software version 10.10.0. The % of killing (ADCC) was calculated using the following formula: ([(% p24+ cells in targets+effectors) – (% p24+ cells in target+effectors+ plasma)]/(% p24+ cells in targets only)) x 100. [78,84]

High-dimensional analysis of flow cytometry data (tSNE and FlowSOM)

For visualising high dimensional flow cytometry data, we used the tSNE nonlinear dimensionality reduction algorithm. For the NK cell phenotype, tSNE maps were generated on NK cells gated on live lymphocytes, using data from the following compensated parameters as input: NKG2C, NKp46, CD57, Granzyme B + Perforin and DNAM-1 and after excluding $CD3^+$ $CD14^+$ $CD19^+$ cells. For the functional analysis, tSNE was performed on $CD107a^+$ NK cells of the concatenated file resulting from three different stimulation conditions (no plasma, HIV+ autologous plasma and HIV+ heterologous plasma) within the same individual. First, the "DownSample" FlowJo plugin was run on NK cells in order to reduce and uniform the population sizes for the further concatenation of samples into a single FCS file, then tSNE maps were generated on $CD107a^+$ NK cells using data from the following compensated parameters as input: IFN-ɣ, NKG2C, NKp46, CD57, Granzyme B + Perforin and DNAM-1.

tSNE settings were the ANNOY algorithm, k nearest neighbors (KNN) algorithm and the Fast Fourier Transform (FTT) Interpolation as gradient algorithm, being tSNE plots less than 5 million events.

In order to visualise marker expression across $CD107a^+$ NK cell subsets of the three selected participants, we run the "FlowSOM" plugin, on the concatenated files. A heatmap displaying the relative expression in each metacluster of each parameter (IFN-ɣ, NKG2C, NKp46, CD57, Granzyme B + Perforin and DNAM-1) used for the FlowSOM analysis was generated (Figure S6).

QUANTIFICATION AND STATISTICAL ANALYSIS

Virological data is presented as column analyses, scatterplots, bar charts and pie charts, with individual values shows as well as median averages, inter-quartile ranges (IQR), and box and whisker charts. Comparative statistical analyses of HIV-1 reservoirs between cohorts was performed on GraphPad Prism. Kruskal-Wallis tests with False Discovery Rate (FDR – Benjamini-Hochberg method) adjusted *p*-values (presented as q-values) were performed on the virology data. For contingency table data, Fishers' exact tests were performed, with *p*-values presented. For xy relationship analysis on ART timing and HIV-1 reservoir data, linear regression analyses were performed, with Spearman's correlations conducted, R^2, *p*-values and rho values are all presented.

Immunological data is presented as column analyses and violin plots, with individual values, median average, and IQRs. Comparative statistical analysis and figure generation was performed using R, with Mann Whitney U, Wilcoxon and paired t-tests used. Correlations between virological and immunological data were conducted in R, with linear regressions and Spearman's correlations performed, R^2, *p*-values and rho values are all presented. High dimensional flow cytometry analyses is described in the Method Details.